Autophagy

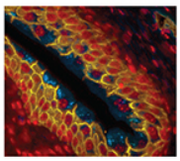

Autophagy

ISSN: 1554-8627 (Print) 1554-8635 (Online) Journal homepage: https://www.tandfonline.com/loi/kaup20

MITF-*MIR211* axis is a novel autophagy amplifier system during cellular stress

Deniz Gulfem Ozturk, Muhammed Kocak, Arzu Akcay, Kubilay Kinoglu, Erdogan Kara, Yalcin Buyuk, Hilal Kazan & Devrim Gozuacik

To cite this article: Deniz Gulfem Ozturk, Muhammed Kocak, Arzu Akcay, Kubilay Kinoglu, Erdogan Kara, Yalcin Buyuk, Hilal Kazan & Devrim Gozuacik (2019) MITF-*MIR211* axis is a novel autophagy amplifier system during cellular stress, Autophagy, 15:3, 375-390, DOI: 10.1080/15548627.2018.1531197

To link to this article: https://doi.org/10.1080/15548627.2018.1531197

AUTOPHAGY
2019, VOL. 15, NO. 3, 375–390
https://doi.org/10.1080/15548627.2018.1531197

Taylor & Francis
Taylor & Francis Group

RESEARCH PAPER - BASIC SCIENCE

MITF-*MIR211* axis is a novel autophagy amplifier system during cellular stress

Deniz Gulfem Ozturk[a], Muhammed Kocak[a], Arzu Akcay[b], Kubilay Kinoglu[b], Erdogan Kara[b], Yalcin Buyuk[b], Hilal Kazan[c], and Devrim Gozuacik [a,d,e]

[a]Sabanci University, Faculty of Engineering and Natural Sciences, Molecular Biology, Genetics and Bioengineering Program, Orhanli-Tuzla, Turkey; [b]Council of Forensic Medicine, Ministry of Justice, Bahcelievler, Turkey; [c]Antalya Bilim University, Faculty of Engineering, Department of Computer Engineering, Antalya, Turkey; [d]Center of Excellence for Functional Surfaces and Interfaces for Nano Diagnostics (EFSUN)Orhanli-Tuzla, Turkey; [e]Sabanci University Nanotechnology Research and Application Center (SUNUM), Sabanci University, Orhanli-Tuzla, Turkey

ABSTRACT

Macroautophagy (autophagy) is an evolutionarily conserved recycling and stress response mechanism. Active at basal levels in eukaryotes, autophagy is upregulated under stress providing cells with building blocks such as amino acids. A lysosome-integrated sensor system composed of RRAG GTPases and MTOR complex 1 (MTORC1) regulates lysosome biogenesis and autophagy in response to amino acid availability. Stress-mediated inhibition of MTORC1 results in the dephosphorylation and nuclear translocation of the TFE/MITF family of transcriptional factors, and triggers an autophagy- and lysosomal-related gene transcription program. The role of family members TFEB and TFE3 have been studied in detail, but the importance of MITF proteins in autophagy regulation is not clear so far. Here we introduce for the first time a specific role for MITF in autophagy control that involves upregulation of *MIR211*. We show that, under stress conditions including starvation and MTOR inhibition, a MITF-*MIR211* axis constitutes a novel feed-forward loop that controls autophagic activity in cells. Direct targeting of the MTORC2 component RICTOR by *MIR211* led to the inhibition of the MTORC1 pathway, further stimulating MITF translocation to the nucleus and completing an autophagy amplification loop. In line with a ubiquitous function, MITF and *MIR211* were co-expressed in all tested cell lines and human tissues, and the effects on autophagy were observed in a cell-type independent manner. Thus, our study provides direct evidence that MITF has rate-limiting and specific functions in autophagy regulation. Collectively, the MITF-*MIR211* axis constitutes a novel and universal autophagy amplification system that sustains autophagic activity under stress conditions.

Abbreviations: ACTB: actin beta; AKT: AKT serine/threonine kinase; AKT1S1/PRAS40: AKT1 substrate 1; AMPK: AMP-activated protein kinase; ATG: autophagy-related; BECN1: beclin 1; DEPTOR: DEP domain containing MTOR interacting protein; GABARAP: GABA type A receptor-associated protein; HIF1A: hypoxia inducible factor 1 subunit alpha; LAMP1: lysosomal associated membrane protein 1; MAP1LC3B/LC3B: microtubule associated protein 1 light chain 3 beta; MAPKAP1/SIN1: mitogen-activated protein kinase associated protein 1; MITF: melanogenesis associated transcription factor; MLST8: MTOR associated protein, LST8 homolog; MRE: miRNA response element; MTOR: mechanistic target of rapamycin kinase; MTORC1: MTOR complex 1; MTORC2: MTOR complex 2; PRR5/Protor 1: proline rich 5; PRR5L/Protor 2: proline rich 5 like; RACK1: receptor for activated C kinase 1; RPTOR: regulatory associated protein of MTOR complex 1; RICTOR: RPTOR independent companion of MTOR complex 2; RPS6KB/p70S6K: ribosomal protein S6 kinase; RT-qPCR: quantitative reverse transcription-polymerase chain reaction; SQSTM1: sequestosome 1; STK11/LKB1: serine/threonine kinase 11; TFE3: transcription factor binding to IGHM enhancer 3; TFEB: transcription factor EB; TSC1/2: TSC complex subunit 1/2; ULK1: unc-51 like autophagy activating kinase 1; UVRAG: UV radiation resistance associated; VIM: vimentin; VPS11: VPS11, CORVET/HOPS core subunit; VPS18: VPS18, CORVET/HOPS core subunit; WIPI1: WD repeat domain, phosphoinositide interacting 1

ARTICLE HISTORY
Received 18 September 2017
Revised 21 September 2018
Accepted 26 September 2018

KEYWORDS
Autophagy; cellular stress; lysosome; microRNA; MITF; MTOR; RICTOR

Introduction

Autophagy is an evolutionarily conserved catabolic pathway that is necessary for the maintenance of cellular homeostasis in eukaryotes [1]. Active at a basal level, autophagy may be upregulated in response to cellular stress conditions, including nutrient (e.g., amino acid) and growth factor deprivation, changes in ATP:ADP ratios, unfolded, misfolded or mutant protein accumulation, oxidative stress and hypoxia, etc [2]. Following autophagy activation, double-membrane compartments termed phagophores are formed in the cytosol, engulfing cytosolic components as well as organelles, such as mitochondria. The phagophores subsequently mature into autophagosomes. Fusion of autophagosomes with lysosomes results in the delivery of autophagy targets to lysosomes, and allows their degradation and recycling [3].

CONTACT Devrim Gozuacik dgozuacik@sabanciuniv.edu Sabanci University. Faculty of Engineering and Natural Sciences, Molecular Biology, Genetics and Bioengineering Program, Orhanli-Tuzla, Istanbul 34956, Turkey; Center of Excellence for Functional Surfaces and Interfaces for Nano Diagnostics (EFSUN)Orhanli-Tuzla, Turkey; Sabanci University Nanotechnology Research and Application Center (SUNUM), Orhanli-Tuzla, Turkey

Supplemental data for this article can be accessed here.

Autophagic activity is regulated by various upstream signaling pathways. The serine/threonine kinase MTOR negatively controls autophagy through inhibitory phosphorylations of the components of the key autophagy-related complex ULK1/2-ATG13 and through regulation of ATG5-RACK1 protein complexes [4,5]. The MTOR kinase is found in 2 different protein complexes: MTOR complex 1 (MTORC1) and MTORC2. MTORC1 is composed of the MTOR kinase and its positive (RPTOR and MLST8) and negative (AKT1S1/PRAS40 and DEPTOR) regulators [6,7]. Conversely, components of MTORC2 include RICTOR, MLST8, DEPTOR, MAPKAP1/SIN1 and PRR5/PROTOR1-PRR5L/PROTOR2 [7,8]. Stability, integrity and function of the MTORC2 complex rely on the presence of various components, including RICTOR [9]. While MTORC2 is primarily regulated by INSR (insulin receptor)-phosphoinositide 3-kinase signaling [10], MTORC1 integrates signals emanating from the STK11/LKB1-AMPK, RAS-MAP2K1/MEK-MAPK1/ERK2-MAPK3/ERK1, WNT and AKT pathways converging at the level of TSC1/2, negative regulators of MTORC1 activity [11,12]. Yet, between these 2 major MTOR complexes crosstalk mechanisms exist and depend on signaling components, including AKT [13].

Another mode of regulation of MTORC1 is through RRAG proteins [14]. Amino acid availability is sensed by RRAG GTPases that control subcellular localization of MTORC1. In the presence of amino acids, MTORC1 complexes are recruited to lysosome membranes through active RRAG GTPase heterodimers (RRAGA/B-GTP and RRAGC/D-GDP), leading to their activation by RHEB proteins [12]. In fact, RRAG GTPases bind and recruit TFEB, TFE3 and MITF transcription factors to lysosomes, promoting their MTORC1-dependent phosphorylation, and their sequestration in the cytosol by YWHA/14–3-3 proteins [15]. Conversely, amino acid starvation shuts-off RRAG proteins, resulting in the inactivation of MTORC1. Under these conditions, the ULK1/2-ATG13 complex is reactivated and can induce autophagy [4]. Moreover, TFEB, TFE3 and MITF transcription factors can be dephosphorylated and then set free to translocate to the nucleus, and stimulate expression of genes coding for autophagy-lysosome components. TFEB, TFE3 and MITF were reported to have partially overlapping autophagy- and lysosome-related targets (Table S1) [16–20]. Whereas the role of TFEB and TFE3 in this context has been studied in detail, whether MITF is indispensable and has a distinct function in autophagy regulation is yet to be established.

Recent studies introduced microRNAs (miRNAs) as new players in the control of autophagy. MiRNAs are 18–21 base pair protein non-coding small RNAs that fine tune cellular levels of transcripts. They do so through modulation of messenger RNA (mRNA) stability and/or through inhibition of protein translation [21]. Indeed, players in various steps of autophagy, including upstream regulatory pathways and core autophagy components, were reported to be targets of different miRNAs [22]. For example, we have previously shown that autophagy-inducing signals upregulated *MIR376A* and *MIR376B* that directly targeted key autophagy genes, ATG4C and BECN1, forming a gas and break mechanism, and preventing uncontrolled and excessive activation of autophagy under prolonged stress conditions [23–25].

Here, we introduce a novel MITF-*MIR211* pathway of autophagy amplification. First, we showed that knockdown of MITF significantly attenuated starvation and MTOR inhibition-mediated autophagy, and established that MITF has a rate-limiting function in autophagy regulation. MITF-dependent control of autophagy required transcriptional activation of its specific target, *MIR211*. Overexpression of *MIR211* potentiated both basal and MTOR-dependent autophagy, and its downregulation resulted in a decrease in the amplitude of autophagy. We determined that the MTORC2 component RICTOR was a rate limiting and direct target of *MIR211*. RICTOR downregulation by *MIR211* attenuated the MTORC1 signal through an AKT-mediated crosstalk, further stimulating MITF translocation to the nucleus. We confirmed co-expression of MITF and *MIR211* in tested cell lines and human tissues. All together, our results showed that a MITF-specific and *MIR211*-dependent feed-forward amplification mechanism is required for optimal autophagy activation under cellular stress conditions.

Results

MITF is required for starvation and MTOR inhibition-induced autophagy

Under basal conditions, TFEB and MITF transcription factors are phosphorylated by MTORC1 and sequestered in the cytosol [15]. Upon MTORC1 inhibition secondary to cellular stress, especially amino acid starvation, both factors migrate to the nucleus, and transactivate several lysosome- and autophagy-related genes. In previous studies, TFEB was introduced as a master regulator of lysosomal biogenesis [26,27]. Although some reports in the literature indicate that MITF contributes to autophagy control, detailed and convincing analyses are missing [15,16,28]. In order to evaluate whether MITF is indispensable for autophagy and that it has a specific function in autophagy regulation, we analyzed MITF function under classical autophagy-inducing conditions.

First, we overexpressed GFP-fused constructs of TFEB and MITF in HeLa cells. Under control conditions, TFEB (Figure S1(a,b)) and MITF (Figures 1(a–d) and S1(c)) proteins were cytosolic, and they were excluded from the nucleus. Upon treatment with autophagy inducers, the MTOR inhibitor torin1 or starvation, both TFEB (Figure S1(a,b)) and MITF (Figures 1(a–d) and S1(c)) translocated to nuclei in almost all analyzed cells as previously reported [29]. To clarify the role of MITF in this context, we analyzed autophagic activity in cells. We tested the effect of the overexpression of MITF-A (an alternative splicing isoform of MITF) in HeLa cells using the LC3 shift assay. In order to clarify whether the observed accumulation of the LC3-II form of the protein was a result of increased autophagic activity, and not a result of a block in autophagosome-lysosome fusion, we performed the experiments in the presence or absence of the lysosomal protease inhibitors E64D-pepstatin A. We observed that, upon treatment with torin1, extracts from cells that overexpressed MITF had higher levels of LC3-II and further accumulation was observed upon lysosomal inhibition confirming that MITF stimulated autophagosome formation and did not

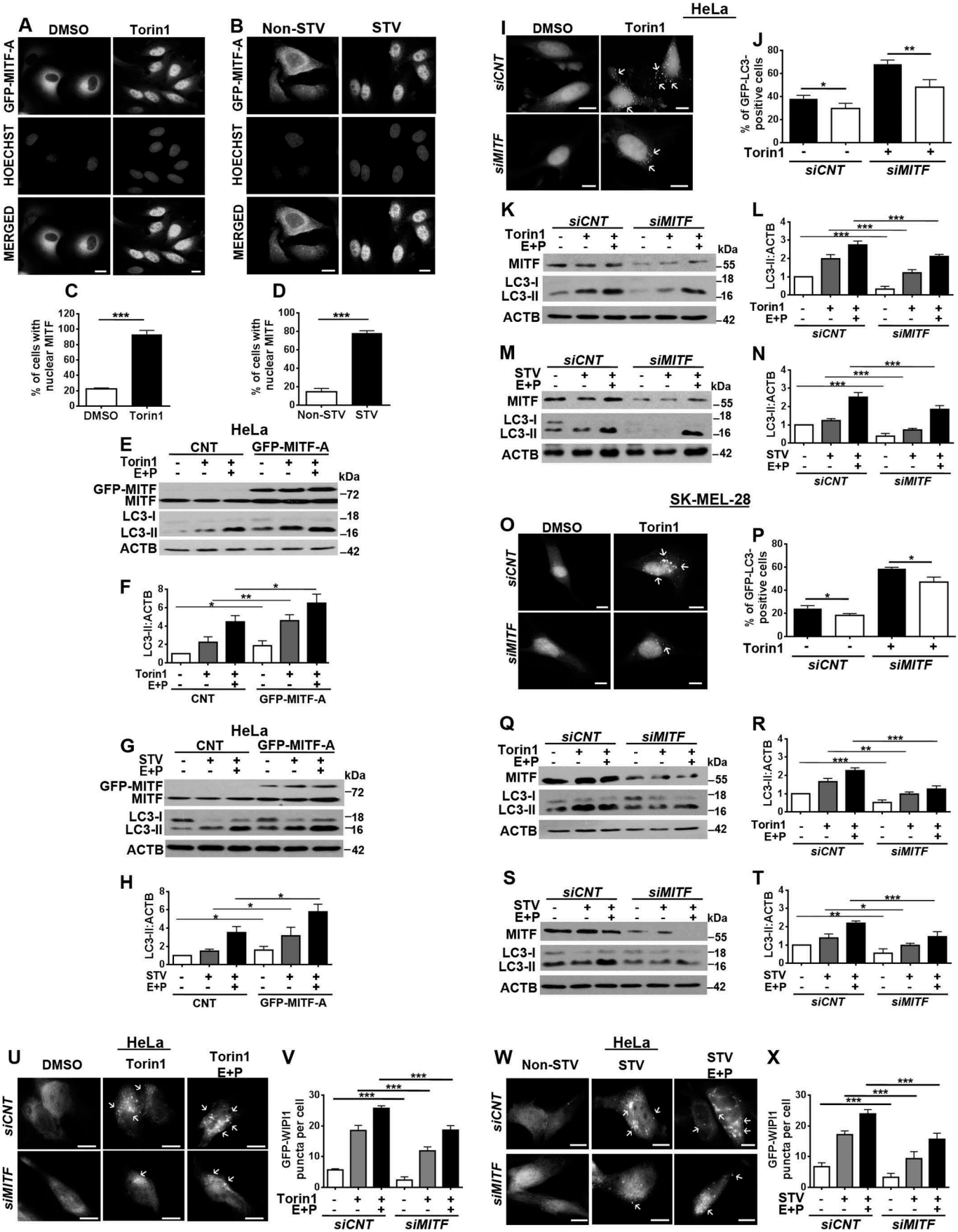
A
DMSO
Torin1
GFP-MITF-A
HOECHST
MERGED
B
Non-STV
STV
C
% of cells with nuclear MITF
DMSO
Torin1
D
Non-STV
STV
HeLa
E
CNT
GFP-MITF-A
Torin1
E+P
kDa
GFP-MITF
MITF
LC3-I
LC3-II
ACTB
F
LC3-II:ACTB
G
STV
H
I
siCNT
siMITF
J
% of GFP-LC3-positive cells
K
L
M
N
SK-MEL-28
O
P
Q
R
S
T
U
V
GFP-WIPI1 puncta per cell
W
X

prominently affect autophagosome-lysosome fusion (Figure 1(e,f)). Similar results were obtained when starvation was used as an autophagy stimulus (Figure 1(g,h)).

To check whether endogenous MITF was a rate-limiting factor in autophagy activation by stress, we transfected cells with siRNAs targeting *MITF* (*siMITF*) or control siRNAs (*siCNT*), and checked autophagy levels under basal conditions or with autophagy inducers and in the presence or absence of the lysosomal inhibitors E64D-pepstatin A. Of note, we confirmed that pan-MITF siRNAs that were used in this study could target all endogenous *MITF* isoforms (Figure S2(a,b)). Moreover, siRNA knockdown of MITF protein levels were confirmed and quantified for each and every experiment and their triple replicates (Figure S2(c–f)). Under these experimental conditions, GFP-LC3 dot formation analysis showed that knockdown of MITF significantly attenuated autophagy that was stimulated by torin1 in HeLa cells (Figure 1(i,j)). Interestingly, MITF downregulation could even suppress autophagy at basal levels (Figure 1(j)). Moreover, MITF-dependence of autophagy was confirmed by LC3-II shift assays that were performed in torin1- (Figure 1(k,l)) or starvation- (Figure 1(m,n)) treated HeLa cells in the presence or absence of E64D-pepstatin A. Additionally, the inhibitory effect of MITF knockdown on torin1-induced autophagy was confirmed in SK-MEL-28 cells (human skin malignant melanoma cell line), using both GFP-LC3 dot formation assays (Figure 1(o,p)). These results were also confirmed in torin1- or starvation-treated SK-MEL-28 cells using LC3-II shift assays (Figure 1(q–t)). During autophagy activation, the phosphatidylinositol-3-phosphate (PtdIns3P) effector WIPI1 proteins are recruited to phagophores and form punctate patterns [30]. In line with LC3 tests, MITF knockdown significantly decreased GFP-WIPI1 dot formation following torin1 treatment (Figure 1(u,v)) or starvation (Figure 1(w,x)). All these results clearly showed that MITF is required for the upregulation of autophagy in cells under stress.

To further confirm that MITF did not block autophagosome-lysosome fusion and increased the autophagic flux, we used 2 independent approaches. The GFP-RFP-LC3 tandem fusion construct is commonly used to assess autophagosome and autolysosome numbers. Whereas GFP and RFP label autophagosomes, the GFP signal quenches in the lysosomes while the RFP signal remains, marking autolysosomes. Quantitative analysis of autophagosome and autolysosome numbers using this test showed that torin1 led to an increase in both autophagosome and autolysosome numbers, and the knockdown of MITF significantly decreased the numbers of both vesicle types (Figure S2(g,h)). Additionally, we used another flux test that was suggested in the autophagy guidelines article [31], the GFP-LC3 lysosomal delivery and proteolysis test. Here, when GFP-LC3 is delivered to lysosomes, the LC3 part of the chimera is degraded, whereas the GFP protein that is relatively resistant to hydrolysis accumulates. Therefore, the appearance of free GFP on western blots can be used to monitor breakdown of the autophagosomal cargo. Using this test, we observed a robust accumulation of free GFP in torin1-treated cells, indicating increased flux and degradation. Knockdown of MITF almost completely abolished free GFP accumulation under these conditions. All of these results showed that MITF is required for autophagic activity in cells (Figure S2(i)). Therefore, MITF is a key regulator of MTOR inhibition- and starvation-induced autophagy.

Role of MITF-dependent transcriptional activation in autophagy control

Previous studies indicated that transcription of some autophagy-related genes, including *LC3B* and *ATG10*, are regulated in a MITF-dependent manner [16,31]. We tested the expression of these autophagy genes following MITF knockdown under control, torin1 or starvation conditions. MITF knockdown significantly attenuated both basal, torin1- (Figure 2(a,b)) or starvation- (Figure 2(c,d)) induced expression of *ATG10* (Figure 2(a,c)) and *LC3B* (Figure 2(b,d)). Using chromatin immunoprecipitation (ChIP) experiments, we confirmed that MITF could bind to the promoter of *LC3B* and, when autophagy was stimulated, MITF binding to the

Figure 1. MITF was required for starvation and MTOR inhibition-induced autophagy. (a and b) MITF translocated to nuclei of cells following torin1 (MTOR inhibitor) (a) or starvation (b) treatment. HeLa cells were transiently transfected with GFP-MITF-A vector and incubated with either torin1 (200 nM, 4 h) or in starvation medium (Earle's Balanced Salt solution, 4 h, STV) and analyzed under a flourescence microscope. DMSO, carrier control. Non-STV, non-starved. Hoechst dye was used to stain the nuclei (blue). Scale bar: 10 μm. (**c and d**) Quantitative analysis of MITF nuclear translocation in the experimental set-up shown in A and B (mean± SD of n = 3 independent experiments, ***p < 0.01). (**e**) Overexpression of MITF-A amplified torin1-induced LC3-II (lipid-conjugated and autophagosome-associated LC3 form) formation in HeLa cells. LC3-I, free LC3 form. E + P, E64D (10 μg/ml) and pepstatin A (10 μg/ml) were used as lysosomal protease inhibitors. (**f**) Graph depicting quantification of LC3-II:ACTB ratios in the experimental set-up shown in E (mean± SD, n = 3 independent experiments, **p < 0.03, *p < 0.05). (**g**) Overexpression of MITF-A increased starvation-induced LC3-II formation in HeLa cells. (**h**) Graph depicting quantification of LC3-II:ACTB ratios in the experimental set-up shown in G (mean± SD, n = 3 independent experiments, *p < 0.05). (**i**) MITF knockdown by *siMITF* attenuated torin1-induced GFP-LC3 puncta formation compared to control siRNA (*siCNT*)-transfected HeLa cells. Scale bar: 10 μm. (**j**) Quantitative analysis of GFP-LC3 dots in the experimental set-up shown in I (mean± SD of n = 3 independent experiments, **p < 0.03, *p < 0.05). (**k**) Immunoblots of *siCNT*- or *siMITF*-transfected HeLa cells that were treated with DMSO or torin1. (**l**) Graph depicting quantification of LC3-II:ACTB ratios in the experimental set-up shown in K (mean± SD, n = 3 independent experiments, ***p < 0.01). (**m**) Immunoblots of *siCNT* or *siMITF* transfected and non-starved or starved HeLa cells. (**n**) Graph depicting quantification of LC3-II:ACTB ratios in the experimental set-up shown in M (mean± SD, n = 3 independent experiments, ***p < 0.01). (**o**) *siMITF* blocked torin1-induced GFP-LC3 puncta formation in SK-MEL-28 cells. Scale bar: 10 μm. (**p**) Quantitative analysis of GFP-LC3 dots in the experimental set-up shown in O (mean± SD of n = 3 independent experiments,*p < 0.05). (**q**) Immunoblots of *siCNT*- or *siMITF*-transfected SK-MEL-28 cells that were treated with DMSO or torin1. (**r**) Graph depicting quantification of LC3-II:ACTB ratios in the experimental set-up shown in Q (mean± SD, n = 3 independent experiments, ***p < 0.01, **p < 0.03). (**s**) Immunoblots of *siCNT*- or *siMITF*-transfected and non-starved or starved SK-MEL-28 cells. (**t**) Graph depicting quantification of LC3-II:ACTB ratios in the experimental set-up shown in S (mean± SD, n = 3 independent experiments, ***p < 0.01, **p < 0.03, *p < 0.05). (**u**) *siMITF* blocked torin1-induced GFP-WIPI1 puncta formation in HeLa cells. Scale bar: 10 μm. (**v**) Quantitative analysis of GFP-WIPI1 puncta in the experimental set-up shown in U (mean± SD of n = 3 independent experiments, ***p < 0.01). (**w**) *siMITF* blocked starvation-induced GFP-WIPI1 puncta formation in HeLa cells. Scale bar: 10 μm. (**x**) Quantitative analysis of GFP-WIPI1 dots in the experimental set-up shown in W (mean± SD of n = 3 independent experiments, ***p < 0.01).

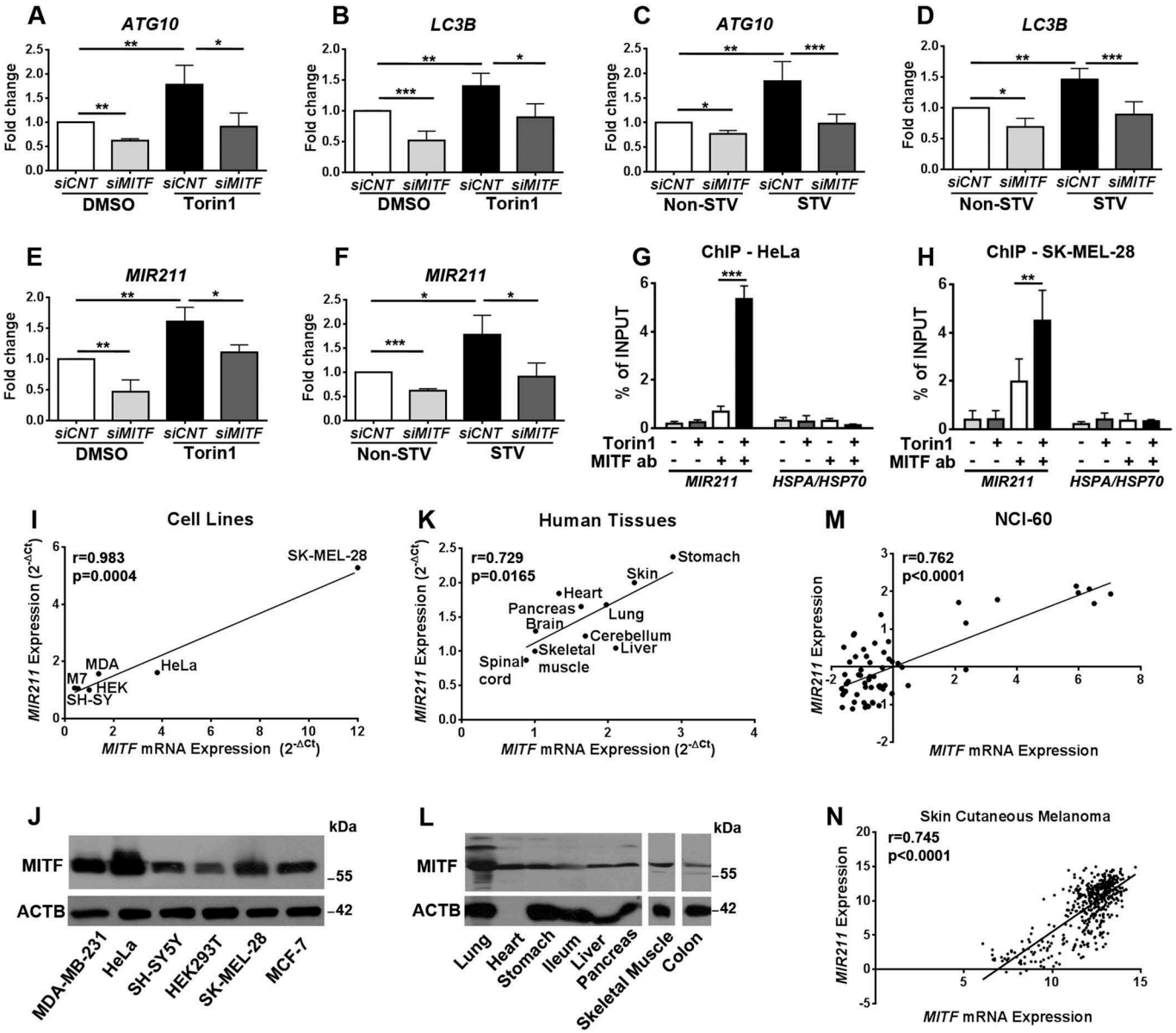

Figure 2. MITF regulated expression levels of autophagy-related genes and *MIR211*. (**a-d**) RT-qPCR analysis of mRNA levels of *ATG10* (a and c) and *LC3B* (b and d) in control siRNA (*siCNT*)- or *siMITF*-transfected HeLa cells following torin1 (a and b) or starvation (c and d) treatment (mean± SD of n = 5 independent experiments ***p < 0.01, **< 0.03, *p < 0.05). DMSO, carrier control. Data were normalized to *GAPDH*. (**e**) TaqMan RT-qPCR analysis of *MIR211* expression in DMSO or torin1-treated HeLa cells (mean± SD of n = 3 independent experiments, **p < 0.03, *p < 0.05). Data were normalized to *RNU6-1* (RNA, U6 small nuclear 1) (U6). (**f**) TaqMan RT-qPCR analysis of *MIR211* expression in non-starved (Non-STV) or starved (STV) HeLa cells (mean± SD of n = 3 independent experiments, ***p < 0.01, *p < 0.05). Data were normalized to *RNU6-1*. (g and h) ChIP assays showing specific association of MITF with the *MIR211* promoter region in HeLa (G) and SK-MEL-28 (H) cells under DMSO or torin1-treated conditions. qPCR results of *MIR211* promoter primers were obtained from input (pre-IP) samples or following ChIP with MITF antibodies. Ct (threshold cycle) ratios were normalized (Ct^{ChIP}/Ct^{input}). In control (CNT) ChIP experiments, no antibody was added. *HSPA/HSP70* promoter primers were used as negative control (mean± SD of n = 3 independent experiments, ***p < 0.01, **p < 0.03). (**i**) Correlation of endogenous *MIR211* and *MITF* mRNA levels in various cell lines. A positive correlation between endogenous *MIR211* and *MITF* mRNA levels was determined by RT-qPCR in MDA-MB-231 (MDA), MCF-7 (M7), SH-SY5Y (SH-SY), HEK293T (HEK), HeLa and SK-MEL-28 cells. r, Pearson's correlation coefficient. (r > 0, positive correlation; p value = 0.004). (**j**) Expression of MITF protein was detected in MDA-MB-231, HeLa, SH-SY5Y, HEK293T, SK-MEL-28, MCF-7 cells using a pan-MITF antibody. (**k**) Correlation of endogenous *MIR211* and *MITF* mRNA levels in human tissues from 4 different cadavers. A positive correlation between endogenous *MIR211* and *MITF* mRNA levels was determined by RT-qPCR in the indicated tissues (Pearson's r coefficient (r) = 0.729, p value (p) = 0.0165). (**l**) Immunoblot analysis of tissue protein extracts from a cadaver using a pan-MITF antibody. ACTB was used as loading control. (**m and n**) The correlation between miRNA and gene expression profile is quantified by computing the correlation coefficient using the NCI-60 expression profiling data (m) (Pearson's r coefficient (r) = 0.762, p value (p)< 0.0001) and TCGA Skin Cutaneous Melanoma (n) (Pearson's r coefficient (r) = 0.745, p value (p)< 0.0001) microRNA and gene expression data.

promoter was significantly increased in 2 different cell lines (Figure S3(a,b)).

Interestingly, a microRNA, *MIR211*, was reported to be a direct transcriptional target of MITF in a melanoma invasion and metastasis context [32,33]. Yet, whether MITF regulates *MIR211* under autophagy-inducing conditions in melanoma and epithelial cells, and whether it contributes to general autophagy control is not known. To confirm that *MIR211* was expressed in HeLa cells, we performed qPCR analysis following control, torin1 or starvation treatment. Torin1

treatment significantly induced *MIR211* expression in HeLa cells (Figure 2(e)). Under these conditions, introduction of *MITF* siRNA significantly decreased both basal and torin1-induced expression of *MIR211* (Figure 2(e)). Similar results were obtained when starvation used was used as an autophagy inducer (Figure 2(f)). Moreover, in ChIP experiments, the amount of MITF protein bound to the *MIR211* promoter region was significantly increased upon autophagy induction by torin1 in HeLa (Figure 2(g)) and SK-MEL-28 (Figure 2(h)) cells. Therefore, all these results showed for the first time that MITF controlled basal and autophagic stress-induced *MIR211* levels in cells.

We also checked that MITF and *MIR211* were co-expressed in several cell lines originating from different tissue types. A positive correlation was found between *MIR211* and *MITF* mRNA expression in cell lines, including HeLa and SK-MEL-28 that were used as cellular models in this study (Figure 2(i)). MITF protein expression in all these cell lines was also demonstrated by immunoblotting analysis (Figure 2(j)). Additionally, analyses of RNAs that were isolated from various human tissues showed a positive correlation between *MIR211* and MITF (Figure 2(k)). MITF protein expression was demonstrated in all studied human tissues as well (Figures 2(l) and S3(c)).

Next, correlation of *MIR211* and MITF expression was checked in publicly available expression datasets: NCI-60 datasets obtained from 60 different cancer cell lines showed that *MIR211* expression positively correlated with MITF expression in these cell lines (Figure 2(m)) ($r = 0.762$, $p < 0.0001$). The Cancer Genome Atlas (TCGA) cancer tissue data subsets were also analyzed. Subsets providing suitable sample size (see Materials and Methods) were skin cutaneous melanoma, pan-kidney cohort, testicular germ cell tumors, glioma and ovarian serous cystadenocarcinoma datasets. While a high correlation of *MIR211*-MITF expression was observed in the skin cutaneous melanoma subset ($r = 0.745$, $p < 0.0001$) (Figure 2(n)), a variable but positive correlation was present in the pan-kidney cohort ($r = 0.11$, $p = 0.0052$), testicular germ cell tumors ($r = 0.26$, $p = 0.0034$) and glioma ($r = 0.22$, $p < 0.0001$) subsets. A similar tendency was observed in the ovarian serous cystadenocarcinoma dataset ($r = 0.13$, $p = 0.0661$) (Figure S3(d–g)).

All of the above data demonstrated for the first time that, in addition to *LC3B* and *ATG10*, MITF regulated *MIR211* expression under autophagy-inducing conditions. Because both MITF and *MIR211* are co-expressed in cell lines and human tissues that were tested in this study, a MITF-*MIR211* axis might play a role in general autophagy control.

MIR211 induced autophagy

In order to test whether *MIR211* stimulated autophagy, we overexpressed miRNA mimic and control constructs in cells (Figure S4(a,b)) and checked for autophagy activation (Figure 3(a–h)). Overexpression of *MIR211* but not the control construct (*MIR-CNT*) induced GFP-LC3 dot formation and LC3 shift in unstimulated HeLa cells in the presence or absence of lysosomal inhibitors (Figure 3(a–d)). Similar results were obtained with SK-MEL-28 cells (Figure 3(e–h)). Moreover, autophagy that was stimulated by torin1 or starvation was further upregulated in both HeLa (Figure 3(i–l)) and SK-MEL-28 (Figure 3(m–p)) cells following *MIR211* overexpression (Figure S4(c–f)). We observed that, following addition of lysosomal inhibitors, LC3-II accumulation was further increased under these conditions upon *MIR211* overexpression (Figure 3(i–p)). Of note, in line with post-translational control of MITF levels under these conditions, there was no significant change in MITF levels upon autophagy stimulation or *MIR211* transfection (Figures S2(c–f) and S5). These results were confirmed using another independent test, a GFP-WIPI1 puncta formation assay following torin1 treatment (Figure 3(q,r)) or starvation (Figure 3(s,t)).

To further provide evidence that *MIR211* stimulated productive autophagy that resulted in autophagosome-lysosome fusion and autophagic flux, we performed quantitative GFP-RFP-LC3 analyses and GFP-LC3 and RFP-LAMP1 colocalization analyses. *MIR211* overexpression stimulated an increase in both autophagosome and autolysosome numbers both in GFP-RFP-LC3 tests (Figure S6(a,b)) and GFP-LC3 and RFP-LAMP1 colocalization analyses (Figure S6(c,d)). All of these data showed that *MIR211* did not block autophagosome-lysosome fusion but rather stimulated autolysosome formation.

Finally, GFP-LC3 lysosomal delivery and proteolysis tests were performed in the presence or absence of lysosomal inhibitors. These analyses showed that *MIR211* stimulated lysosome-dependent degradation of GFP-LC3. Free GFP accumulation was observed following *MIR211* overexpression, whereas inhibition of lysosomal proteases prominently decreased this accumulation (Figure S6(e,f)).

Therefore, *MIR211* stimulated autophagosome and autolysosome formation and autophagic flux.

Inhibition of MIR211 by antagomirs suppressed starvation- and MTOR-dependent autophagy

To reveal the importance of endogenous *MIR211* in autophagy regulation, we inhibited endogenous miRNAs using chemically synthesized anti-*MIR211* antagomir oligonucleotides (*ANT211*) or control oligonucleotides (*ANT-CNT*), and checked torin1- or starvation-induced autophagy in the presence or absence of E64D-pepstatin A. Introduction of *ANT211* led to a decrease in GFP-LC3 dot numbers following torin1 treatment in HeLa (Figure 4(a,b)) and SK-MEL-28 cells (Figure 4(c,d)). In line with these results, torin1-induced LC3-II accumulation was attenuated in *ANT211*-transfected cells compared to the control in both HeLa (Figure 4(e,f)) and SK-MEL-28 (Figure 4(g,h)) cells. When starvation was used as an autophagy inducer, the level of LC3-II decreased in *ANT211*-transfected cells compared to control transfected counterparts in both HeLa (Figure 4(i,j)) and SK-MEL-28 cells (Figure 4(k,l)). *MIR211*-dependence of classical (starvation- or torin1-induced) autophagy was also confirmed using GFP-WIPI1 puncta formation tests (Figure 4(m–p)). These results indicate that endogenous *MIR211* levels are critical cellular factors regulating autophagy activation.

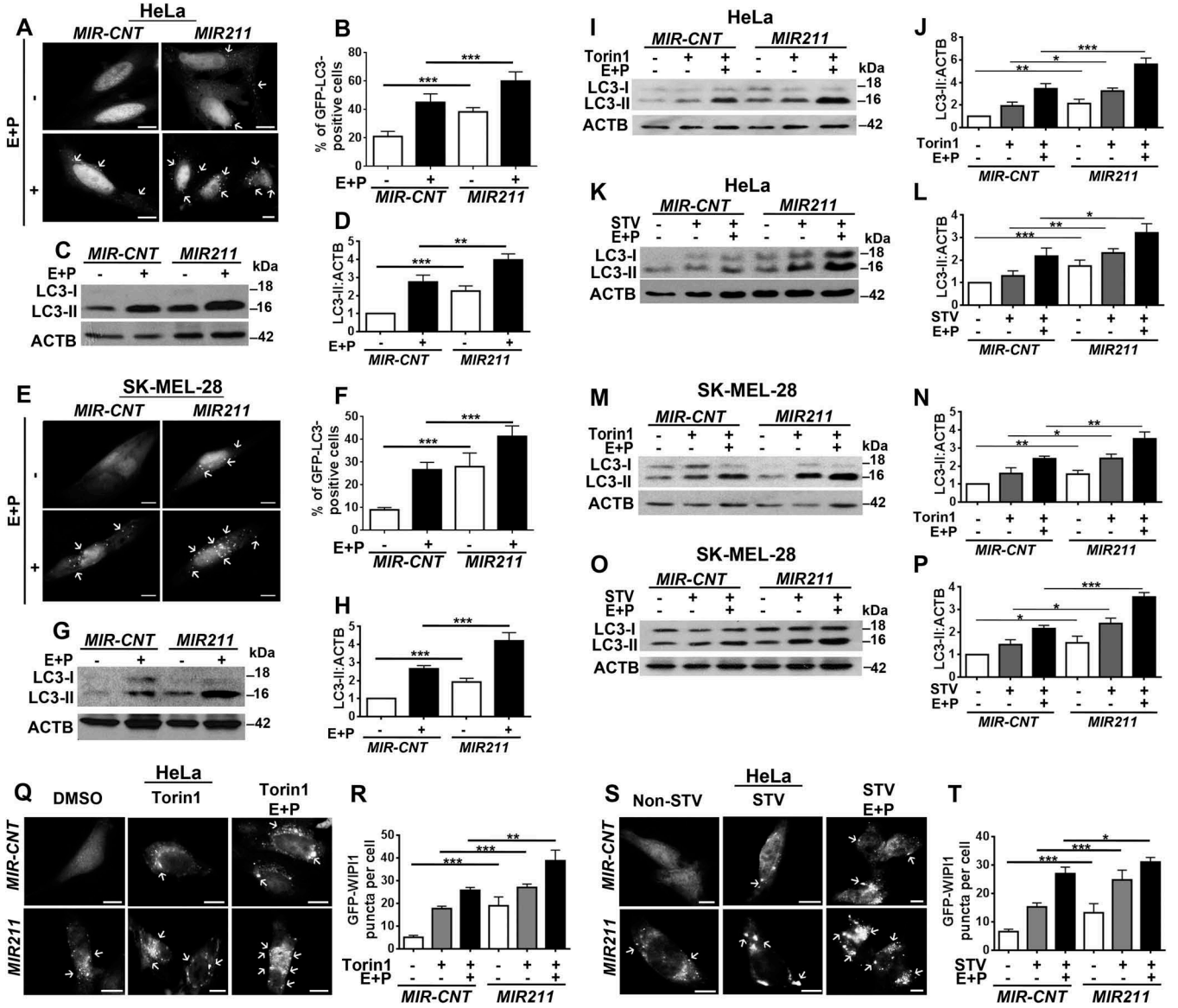

Figure 3. *MIR211* activated autophagy. (**a-d**) Hela cells were transfected with *MIR211* or a control construct (*MIR-CNT*), and autophagy was assessed in the presence and absence of lysosomal inhibitors. (a) *MIR211* overexpression increased GFP-LC3 dot formation. Scale bar: 10 μm. (b) Quantitative analysis of GFP-LC3 dots in the experimental set-up shown in A (mean± SD of n = 3 independent experiments, ***p < 0.01). (c) Autophagy-related LC3-II levels were analyzed in immunoblots of *MIR-CNT*-or *MIR211*-overexpressing HeLa cell extracts. (d) Graph depicting quantification of LC3-II:ACTB ratios in the experimental set-up shown in C (mean± SD, n = 3 independent experiments, ***p < 0.01, **p < 0.03). (**e-h**) *MIR211* overexpression induced autophagy in SK-MEL-28 cells in the presence or absence of lysosomal inhibitors. (e) *MIR211* overexpression increased GFP-LC3 dot formation. Scale bar: 10 μm. (f) Quantitative analysis of GFP-LC3 dots in the experimental set-up shown in E (mean± SD of n = 3 independent experiments, ***p < 0.01). (g) Autophagy-related LC3-II levels were analyzed in immunoblots of *MIR-CNT*-or *MIR211*-overexpressing SK-MEL-28 cell extracts. (h) Graph depicting quantification of LC3-II:ACTB ratios in the experimental set-up shown in G (mean± SD, n = 3 independent experiments, ***p < 0.01). (**i-l**) *MIR211* amplified torin1- or starvation-induced autophagy in HeLa cells. (i) Immunoblots of *MIR-CNT*- or *MIR211*-transfected HeLa cells treated with DMSO or torin1. E + P, E64D and pepstatin A. (j)Graph depicting quantification of LC3-II:ACTB ratios in the experimental set-up shown in I (mean± SD, n = 4 independent experiments, ***p < 0.01, **< 0.03, *p < 0.05). (k) Immunoblots of *MIR-CNT*- or *MIR211*-transfected and non-starved or starved (STV) HeLa cells. (l) Graph depicting quantification of LC3-II:ACTB ratios in the experimental set-up shown in K (mean± SD, n = 3 independent experiments, ***p < 0.01, **p < 0.03, *< 0.05). (**m-p**) *MIR211* amplified torin1- or starvation-induced autophagy in SK-MEL-28 cells. (m) Immunoblots of *MIR-CNT*- or *MIR211*-transfected SK-MEL-28 cells treated with DMSO or torin1. (n) Graph depicting quantification of LC3-II:ACTB ratios in the experimental set-up shown in M (mean± SD, n = 5 independent experiments, ***p < 0.01, **p < 0.03, *p < 0.01). (o) Immunoblots of *MIR-CNT*- or *MIR211*-transfected and non-starved or starved SK-MEL-28 cells. (p) Graph depicting quantification of LC3-II:ACTB ratios in the experimental set-up shown in O (mean± SD, n = 4 independent experiments, ***p < 0.01, *p < 0.05). (**q**) *MIR211* amplified torin1-induced GFP-WIPI1 puncta formation in HeLa cells. Scale bar: 10 μm. (**r**) Quantitative analysis of GFP-WIPI1 puncta in the experimental set-up shown in Q (mean± SD of n = 3 independent experiments, ***p < 0.01, **p < 0.03). (**s**) *MIR211* amplified starvation-induced GFP-WIPI1 puncta formation in HeLa cells. Non-STV, non-starved. STV, starved. Scale bar: 10 μm. (**t**) Quantitative analysis of GFP-WIPI1 puncta in the experimental set-up shown in S (mean± SD of n = 3 independent experiments, ***p < 0.01, *p < 0.05).

RICTOR was an autophagy-related target of MIR211

We next searched for an autophagy-related target(s) of *MIR211* using the bioinformatics tools miRanda, FindTar3, TargetScan, miRDB and RNA22. All of these tools identified *RICTOR* (GenBank accession number: NM_152756) as a potential direct target of *MIR211*. Indeed, we could identify a *MIR211* miRNA response element (MRE) in the 3′ UTR of the *RICTOR* mRNA (Base numbers: 4343–4349, Figure 5(a)).

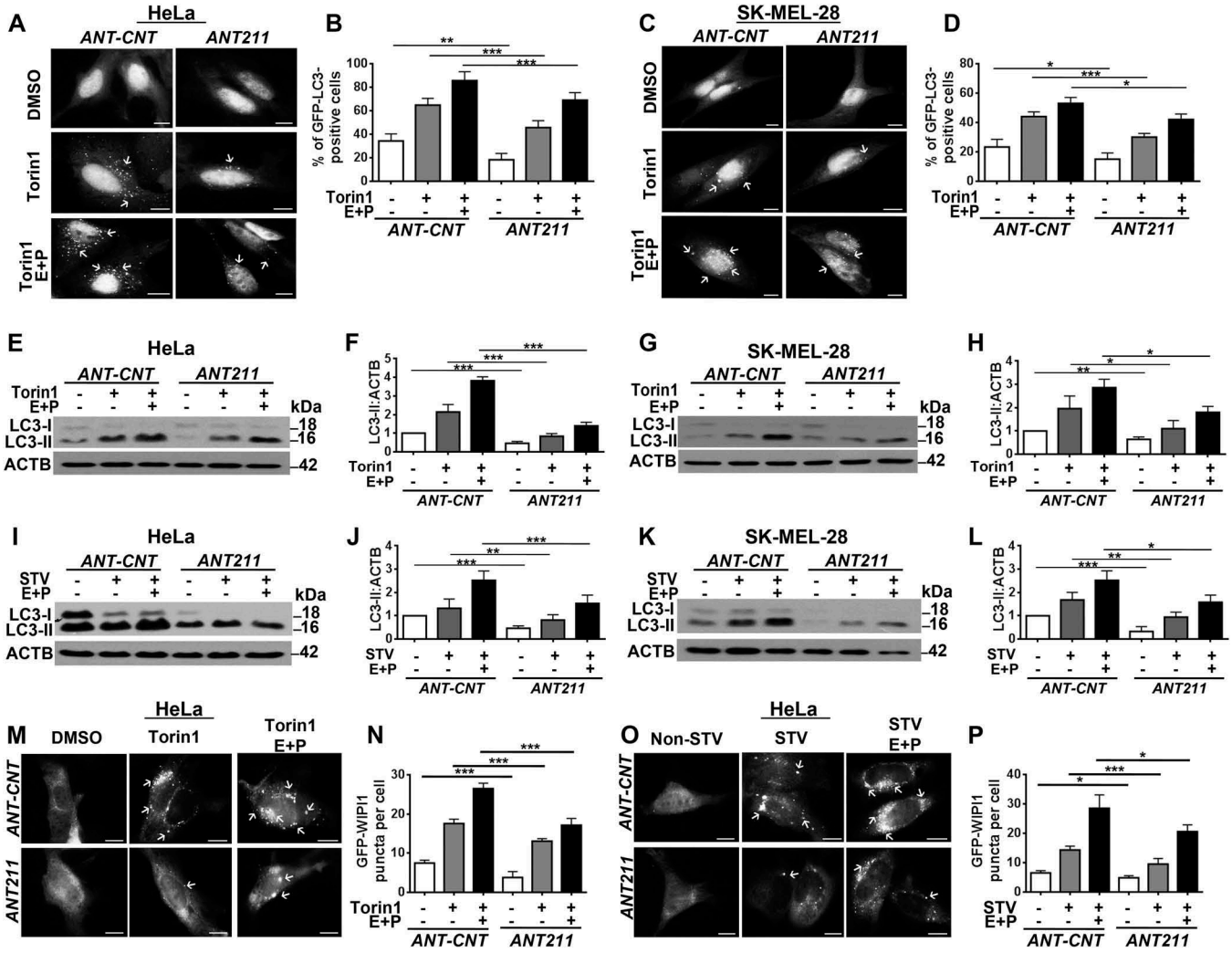

Figure 4. Antagomir-mediated inhibition of *MIR211* led to the suppression of torin1- and starvation-induced autophagy. (**a**) Antagomir against *MIR211* (*ANT211*), but not the control antagomir (*ANT-CNT*), decreased torin1-induced GFP-LC3 puncta formation in the presence or absence of lysosomal inhibitors E64D and pepstatin A (E + P) in HeLa cells. Scale bar: 10 μm. (**b**) Quantitative analysis of GFP-LC3 dots in the experimental set-up shown in A (mean± SD of n = 3 independent experiments, ***p < 0.01, **p < 0.03). (**c**) *MIR211* knockdown by *ANT211* decreased torin1-induced GFP-LC3 puncta formation compared to *ANT-CNT* control in SK-MEL-28 cells. Scale bar: 10 μm. (**d**) Quantitative analysis of GFP-LC3 dots in the experimental set-up shown in C (mean± SD of n = 3 independent experiments, ***p < 0.01, *p < 0.05). (**e**) Immunoblots of *ANT-CNT*- or *ANT211*-transfected HeLa cells that were treated with DMSO or torin1. (**f**) Graph depicting quantification of LC3-II:ACTB ratios in the experimental set-up shown in E (mean± SD, n = 3 independent experiments, ***p < 0.01). (**g**) Immunoblots of *ANT-CNT*- or *ANT211*-transfected SK-MEL-28 cells that were treated with DMSO or torin1. (**h**) Graph depicting quantification of LC3-II:ACTB ratios in the experimental set-up shown in G (mean± SD, n = 3 independent experiments, **p < 0.03, *p < 0.05). (**i**) Immunoblots of *ANT-CNT*- or *ANT211*-transfected and non-starved or starved (STV) HeLa cells. (**j**) Graph depicting quantification of LC3-II:ACTB ratios in the experimental set-up shown in I (mean± SD, n = 3 independent experiments, ***p < 0.01, **p < 0.03). (**k**) Immunoblots of ANT-*CNT*- or *ANT211*-transfected and non-starved or starved SK-MEL-28 cells. (**l**) Graph depicting quantification of LC3-II:ACTB ratios in the experimental set-up shown in K (mean± SD, n = 3 independent experiments, ***p < 0.01, **p < 0.03, *p < 0.05). (**m**) *ANT211* blocked torin1-induced GFP-WIPI1 puncta formation in HeLa cells. Scale bar: 10 μm. (**n**) Quantitative analysis of GFP-WIPI1 puncta in the experimental set-up shown in M (mean± SD of n = 3 independent experiments, ***p < 0.01). (**o**) *ANT211* blocked starvation-induced GFP-WIPI1 puncta formation in HeLa cells. Scale bar: 10 μm. (**p**) Quantitative analysis of GFP-WIPI1 dots in the experimental set-up shown in O (mean± SD of n = 3 independent experiments, ***p < 0.01, *p < 0.05).

In line with these observations, *MIR211* overexpression resulted in the downregulation of *RICTOR* transcript levels in both HeLa and SK-MEL-28 cells (Figure 5(b)). Moreover, overexpression of the miRNA (Figure S4(g,h)) decreased RICTOR protein levels (Figure 5(c,d)), and downregulation of endogenous *MIR211* using antagomirs (Figure S4(g,h)) resulted in the accumulation of RICTOR protein compared to controls (Figure 5(e,f)). Therefore, RICTOR levels in cells are regulated by *MIR211*.

To confirm that the MRE sequence in the 3′UTR of *RICTOR* mRNA was responsive to *MIR211*, we cloned the MRE sequence into the 3′UTR region of the luciferase gene. Additionally, we created a mutant version of this construct by introducing base changes to putative miRNA binding residues (Figure 5(g)). Co-transfection of *MIR211* together with the wild-type luciferase construct into HEK293T (Figure S7(a)), HeLa (Figure 5(h)) and SK-MEL-28 (Figure 5(i)) cells resulted in a significant decrease in luciferase activity. In contrast, *MIR211* could no longer affect luciferase levels when the mutant construct was co-transfected instead (Figures 5(h,i), S7(a)). Therefore, *MIR211* suppressed RICTOR expression through direct binding to its 3′UTR. Similar experiments were performed after transfection of cells with *ANT211*. In line with suppression of endogenous *MIR211* by *ANT211*, a

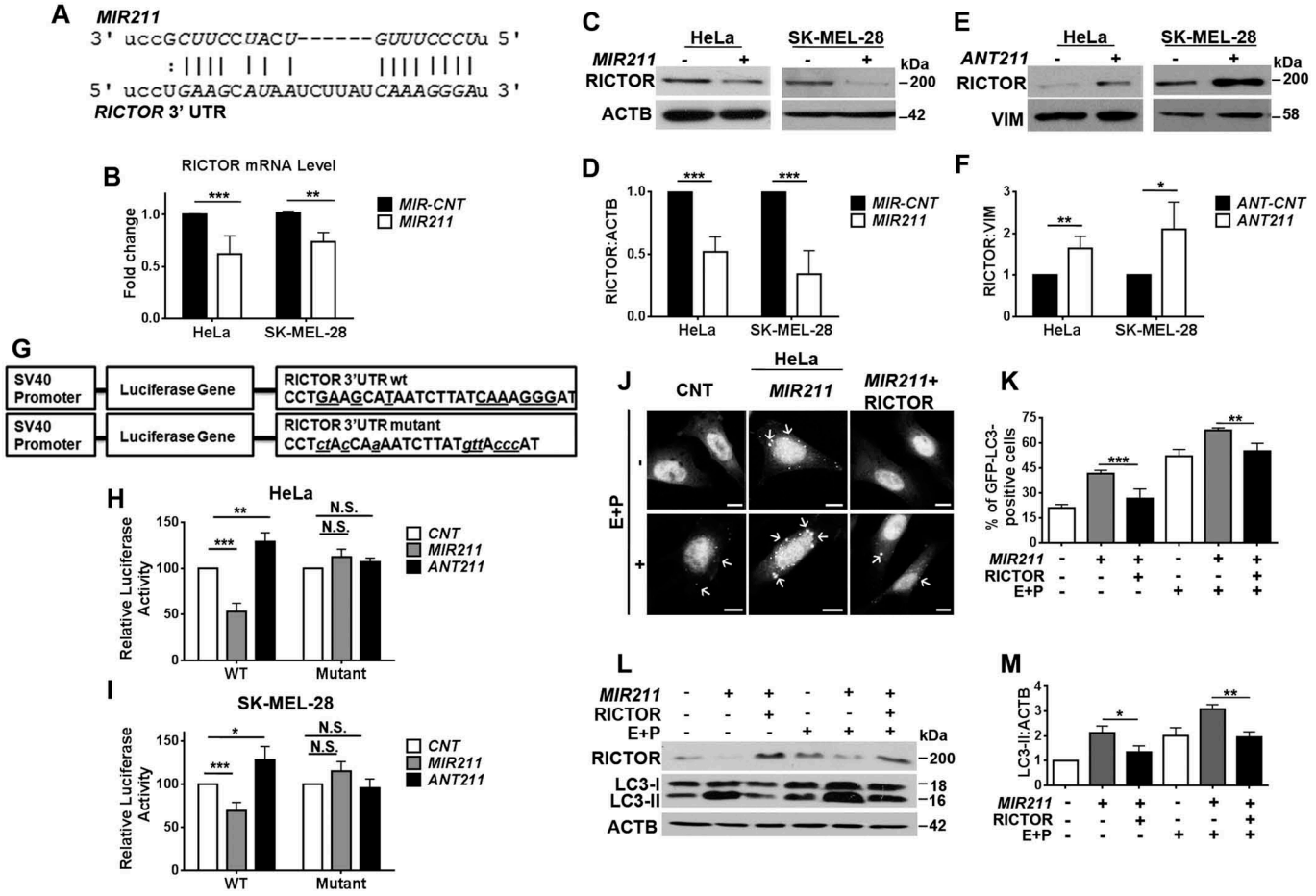

Figure 5. RICTOR was an autophagy-related direct and rate-limiting target of *MIR211*. (**a**) *MIR211* target sequence in the 3′ UTR of *RICTOR* mRNA. The *MIR211* seed sequence was marked in *italics*. (**b**) RT-qPCR analysis of *RICTOR* mRNA levels in control (*MIR-CNT*)- or *MIR211*-transfected HeLa or SK-MEL-28 cells (mean± SD, n = 3 independent experiments, **p < 0.03, ***p < 0.01). Data were normalized using *GAPDH* mRNA as a control. (**c**) Immunoblots of *MIR-CNT* or *MIR211* transfected cells. RICTOR protein levels decreased following *MIR211* overexpression in HeLa or SK-MEL-28 cells. (**d**) Graph depicting quantification of RICTOR:ACTB ratios in the experimental set-up shown in C (mean± SD, n = 3 independent experiments, ***p < 0.01). (**e**) RICTOR protein levels were increased following *ANT211*- but not control antagomir (*ANT-CNT*)-transfection in HeLa and SK-MEL-28 cells. (**f**) Graph depicting quantification of RICTOR:VIM ratios in the experimental set-up shown in E (mean± SD, n = 3 independent experiments, *p < 0.05, **p < 0.03). (**g**) A scheme representing luciferase constructs with wild-type (WT) or mutant *MIR211* target 3′ UTR MRE sequences of *RICTOR*. Mutations were marked in lowercase letters. (**h and i**) Normalized luciferase activity in lysates from HeLa (H) and SK-MEL-28 (I) cells that were co-transfected with wild-type or mutant RICTOR-luciferase constructs and *MIR211* or *ANT211* (mean ± SD of independent experiments, n = 4, *p < 0.05, **p < 0.03, ***p < 0.01, N.S., not significant). (**j**) RICTOR overexpression was sufficient to revert *MIR211*-mediated autophagy induction. HeLa cells were co-transfected with *MIR211* or *MIR-CNT* and a RICTOR expression plasmid lacking the *MIR211* target MRE region (*MIR211*-resistant RICTOR plasmid). GFP-LC3 dot formation was evaluated in the presence or absence of E64D and pepstatin A (E + P). Scale bar: 10 μm. (**k**) Quantitative analysis of GFP-LC3 dots in the experimental set-up shown in J (mean± SD of n = 3 independent experiments, ***p < 0.01, **p < 0.03). (**l**) Immunoblots of extracts from cells transfected with *MIR-CNT, MIR211* or *MIR211* together with the *MIR211*-resistant RICTOR expression plasmid. (**m**) Graph depicting quantification of LC3B:ACTB ratios in the experimental set-up shown in L (mean ± SD, n = 3 independent experiments, **< 0.03, *p < 0.05).

significant increase above control levels was observed in the luciferase activity of *ANT211*-transfected cells, while this effect was not observed in cells transfected with the mutant construct (Figure 5(h,i)).

MicroRNAs may target more than one gene and usually dozens of genes at once. Rescue experiments were performed to validate that RICTOR downregulation was responsible for the autophagy-related effects of *MIR211*. For this purpose, RICTOR protein was overexpressed from a plasmid lacking the MRE region, and therefore resistant to miRNA-mediated silencing. GFP-LC3 puncta formation assays were performed in the presence or absence of E64D-pepstatin A. Under these conditions, *MIR211*-induced autophagy could be suppressed by reintroduction of the RICTOR protein (Figure 5(j,k)). In line with these results, an increase in LC3-II protein levels that was observed upon *MIR211* overexpression (Figure S4(i)), was attenuated when the RICTOR protein was reintroduced, and these effects were enhanced by lysosomal inhibitors (Figure 5 (l,m)). Therefore, expression of RICTOR alone was sufficient for autophagy suppression even in the presence of elevated *MIR211* levels. The above presented data demonstrated for the first time that RICTOR is a rate-limiting target of the MITF-regulated microRNA *MIR211*, in the context of autophagy.

MIR211 regulated the MTORC1 pathway through RICTOR

MTORC2 was directly linked to MTORC1 regulation and autophagy control through AKT phosphorylation. The serine 473 (Ser473) residue on the AKT protein was identified as a direct target of the MTORC2-associated MTOR Ser/Thr kinase [34]. Because we established that RICTOR, a major regulator of MTORC2 activity, was directly down-regulated by *MIR211*, we checked whether AKT Ser473

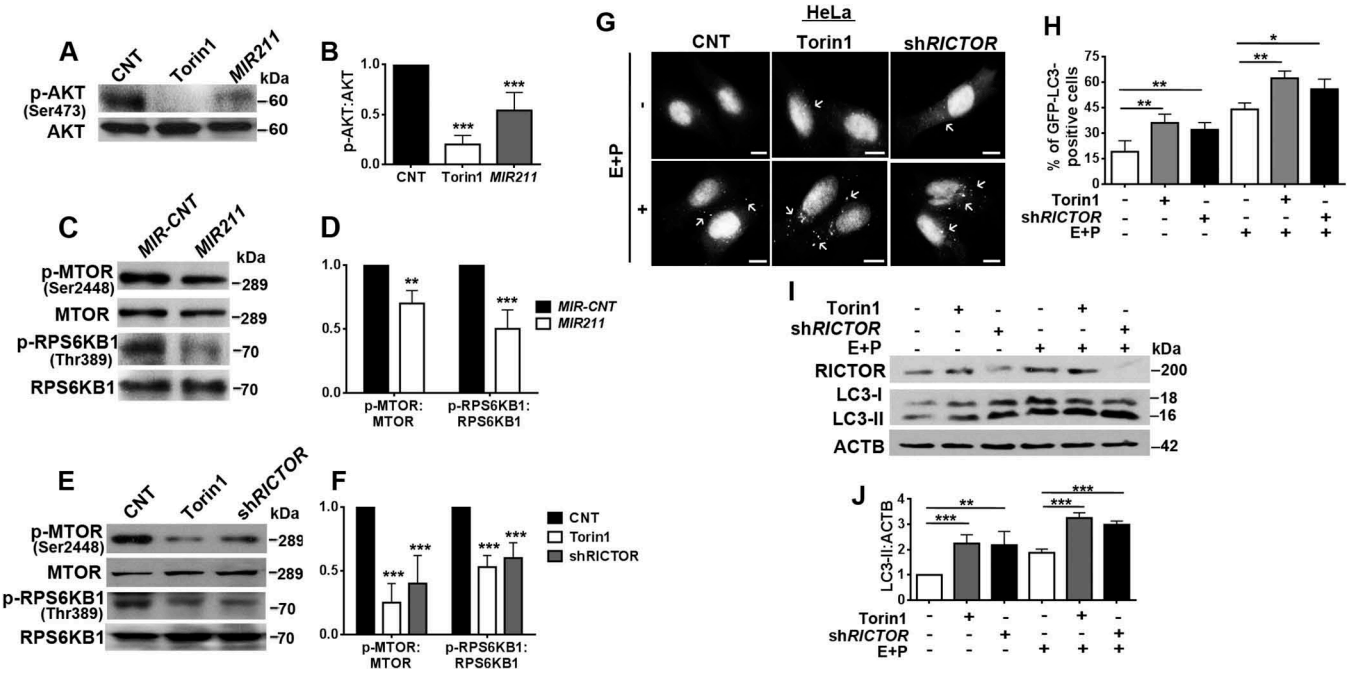

Figure 6. *MIR211* regulated the MTORC1 pathway through RICTOR. (**a**) MTORC2-mediated AKT Ser473 phosphorylation was decreased in HeLa cells overexpressing *MIR211*. Torin1 was used as a positive control. (**b**) Graph depicting quantification of p-AKT:AKT ratios in the experimental set-up shown in A (mean± SD, n = 3 independent experiments, ***p < 0.01). (**c**) MTOR phospho-Ser2448 (p-MTOR) and RPS6KB1 phospho-Thr389 levels were decreased following *MIR211* overexpression in HeLa cells. (**d**) Graph depicting quantification of p-MTOR:MTOR and p-RPS6KB1:RPS6KB1 ratios in the experimental set-up shown in C (mean± SD, n = 3 independent experiments, ***p < 0.01, **< 0.03). (**e**) Knockdown of RICTOR by shRNA (sh*RICTOR*) decreased p-MTOR and p-RPS6KB1 levels. Torin1, positive control. (**f**) Graph depicting quantification of p-MTOR:MTOR and p-RPS6KB1:RPS6KB1 ratios in the experimental set-up shown in E (mean± SD, n = 3 independent experiments, ***p < 0.01). (**g**) Knockdown of RICTOR increased GFP-LC3 dot formation. Torin1, positive control. E + P, E64D and pepstatin A. Scale bar: 10 µm. (**h**) Quantitative analysis of GFP-LC3 dots in the experimental set-up shown in G (mean± SD of n = 3 independent experiments, **p < 0.03, *p < 0.05). (**i**) Immunoblots of LC3-II formation following knockdown of RICTOR. Torin1, positive control. (**j**) Graph depicting quantification of LC3B:ACTB ratios in the experimental set-up shown in I (mean± SD, n = 3 independent experiments, ***p < 0.01, **p < 0.03).

phosphorylation was affected by overexpression of the miRNA. Figure 6(a,b) show that *MIR211* overexpression prominently decreased AKT phosphorylation. In the same experimental context, *MIR211* overexpression blocked the activation of MTORC1 by AKT through MTOR Ser2448 phosphorylation (Figure 6(c,d)). Furthermore, the miRNA also led to a decrease in RPS6KB1 phosphorylation by MTORC1 at Thr389, confirming the inhibition of MTORC1 activity under these conditions (Figure 6(c,d)). We also showed in our system that RICTOR downregulation *per se* was responsible for MTORC1 inhibition by the miRNA. Indeed, introduction of an shRNA against *RICTOR* (sh*RICTOR*) resulted in MTOR Ser2448 and RPS6KB1 Thr389 dephosphorylation, and hence MTORC1 inhibition (Figure 6(e,f)). Moreover, overexpression of RICTOR from a *MIR211*-resistant construct increased MTORC2-related AKT phosphorylation (Figure S7(b)).

Next, we explored autophagy-related consequences of MTORC1 inhibition secondary to RICTOR downregulation. Indeed, transfection of sh*RICTOR* alone stimulated autophagy (Figures 6(g,h), S7(c)). Considering that the knockdown efficiency was approximately 50%, we can conclude that sh*RICTOR* activated autophagy to a comparable level as MTORC1 and MTORC2 inhibitor torin1 treatment (Figure 6(i,j)). All of these data led us to conclude that *MIR211*-mediated RICTOR downregulation resulted in a strong inhibition of the MTORC2-AKT-MTORC1 pathway, leading to the stimulation of autophagy.

MIR211 overexpression resulted in MITF translocation to the nucleus

As previously shown, inhibition of MTORC1 led to the translocation of TFEB and MITF to the nucleus under autophagy-inducing stress conditions (Figures 1(a–d), S1 and as shown in reference [15]). Having demonstrated that *MIR211* led to the inhibition of MTORC1, we wondered whether mere overexpression of the miRNA would lead to a similar outcome. We observed that following *MIR211* overexpression, endogenous TFEB and MITF proteins translocated to the nuclei in a significant fraction of cells (Figure 7(a–d)). Of note, miRNA transfection efficiency was approximately 60% for HeLa cells, indicating that translocation occurred in most of the transfected cells (Figure 7(c,d)). *MIR211*-dependent regulation of MITF nuclear translocation was also observed in other cell lines that were tested (see Figure S8 for results of HEK293T, MCF-7 and SK-MEL-28 cell lines that are derived from different tissue types).

Discussion

Results presented in this article demonstrated that MITF plays a crucial role in starvation and MTOR-inhibition mediated autophagy. In addition to controlling the expression of

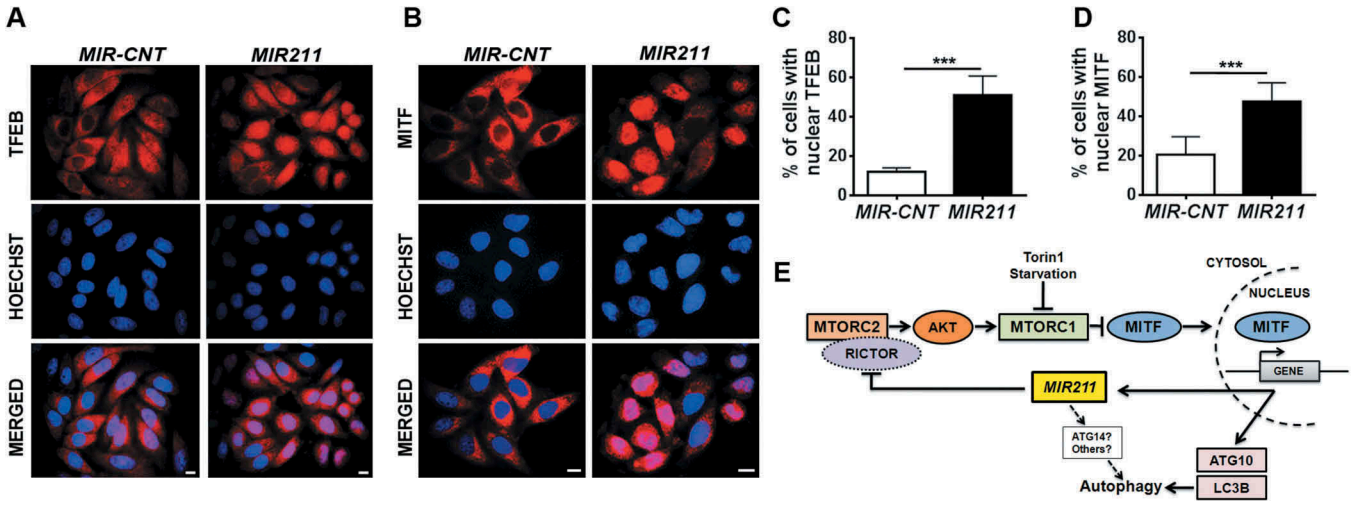

Figure 7. *MIR211* overexpression led to MITF translocation to the nucleus. (**a and b**) Endogenous TFEB (A) or MITF (B) intracellular localizations were analyzed using indirect immunostaining with specific antibodies in HeLa cells transfected with *MIR-CNT* or *MIR211*. Scale bar: 10 µm. (**c and d**) Quantification of endogenous TFEB (c) or MITF (d) nuclear localization (mean± SD, n = 3 independent experiments, ***p < 0.01). (**e**) A model depicting the MITF-*MIR211* autophagy feed-forward regulation pathway. Downregulation of RICTOR by *MIR211* blocks MTORC2 activity, leading to AKT inhibition that is followed by MTORC1 blockage. Under these conditions, MITF that was sequestered in the cytosol migrates to the nucleus and contributes to the transactivation of autophagy-related genes as well as *MIR211*. Upregulation of the miRNA under these conditions creates a feed-forward loop that amplifies and sustains autophagy during stress. Although, we have shown here that RICTOR was a direct and rate-limiting target of *MIR211* in autophagy control (see the rescue assays in Figure 5(j)), additional direct or indirect connections involving other *MIR211* targets (e.g., *ATG14*) might also be contributing to the further amplification of the autophagic activity.

lysosome-related genes, we showed that MITF is a key regulator of autophagic signal amplification through a MITF-*MIR211* axis. We showed that: *i*. Following autophagy-inducing stress, TFEB as well as MITF translocated to the nuclei of cells. *ii*. MITF knockdown significantly downregulated the amplitude of autophagy that was activated by starvation and torin1. *iii*. MITF overexpression potentiated starvation- and torin1-stimulated autophagy. *iv*. Following translocation to the nuclei, MITF transactivated autophagy-related targets as well as *MIR211* expression. *v*. Both MITF and *MIR211* were co-expressed in tested cell lines, human tissue samples and in various tumor datasets. *vi*. Overexpression of *MIR211* stimulated autophagosome and autolysosome formation, and autophagic degradation. *vii*. Knockdown of endogenous *MIR211* limited the increase in the amplitude of autophagy under these conditions, indicating a key role for this miRNA in autophagy regulation. *viii*. *MIR211* overexpression was sufficient for the stimulation of TFEB and MITF translocation to nuclei, and it did so through direct targeting of RICTOR and inhibition of the MTORC2 and MTORC1 pathways. All of these data demonstrated that MITF is a universal amplifier of the autophagy signal in cells, through a feed-forward mechanism involving the MITF-*MIR211*-RICTOR-MTORC1 axis (Figure 7(e)).

MITF is a member of the MITF/TFE family of bHLH-Zip transcription factors, that include TFEB, TFEC, and TFE3. Studies until now implicated TFEB, and to a certain extent TFE3, in the transcriptional regulation of autophagosome and lysosome biogenesis via activation of the genes of crucial proteins, including subunits of the v-ATPase, lysosomal transporters and hydrolases (Table S1). Additionally, some autophagy-related genes such as *BECN1, WIPI, GABARAP, HIF1A, VPS11* and *VPS18* were also reported to be transcriptional targets of TFEB [16,17,20]. Similar to TFEB, TFE3 was shown to perform overlapping gene regulatory functions [16,19]. In contrast, study of MITF function in an autophagy context was limited to the analysis of MITF transcriptional targets, and most studies in the literature on MITF concentrated on its function in melanocyte differentiation and melanoma invasion [35]. Although MITF was shown to regulate a number of overlapping genes with TFEB and TFE3, including autophagy genes *LC3B, ATG10, ATG16L1, SQSTM1, ATG9B* and *UVRAG* (Table S1), whether MITF played a non-redundant and specific function in autophagy regulation was not established so far. Strikingly, none of the studies that were published to date clearly showed the importance of independent contribution of MITF to autophagy regulation. Therefore, our study establishes for the first time a MITF-specific role in autophagic control through a feed-forward autophagy amplification loop involving a MITF-*MIR211* axis.

Transcriptional activation of *MIR211* by MITF was previously reported in a melanoma invasion and metastasis context [32,33,36]. Here, we confirmed that *MIR211* expression was dependent on MITF expression because MITF moved to the nuclei and bound to the *MIR211* promoter under autophagy-stimulating conditions. Furthermore, knockdown of MITF led to a drop in endogenous *MIR211* levels. Conversely, antagomir-mediated silencing of *MIR211* limited the increase in the amplitude of autophagy when MITF was overexpressed, demonstrating the critical role of this miRNA in MITF-dependent autophagy regulation (Figure S9(a,b)).

During the osteogenic differentiation of human induced pluripotent stem cells, a correlation between *MIR211* expression and ATG14 upregulation was suggested, but relevance of this observation for autophagy regulation so far remained obscure [37]. Here, RICTOR was identified as a direct and rate-limiting target of *MIR211* in an autophagy context because the 3′UTR region of the gene contained a *MIR211*-

responsive sequence element, and, in rescue assays, reintroduction of RICTOR protein attenuated autophagy activation by the miRNA. Importantly, we showed that RICTOR downregulation by *MIR211* or specific shRNA, led to a decrease in AKT Ser473 phosphorylation and MTORC1 pathway inhibition. Under these conditions, TFEB and MITF translocated to the nuclei of cells, further increasing *MIR211* levels in a MITF-dependent manner, and activating a gene expression program that determines the amplitude of the autophagic signal.

Up to now, 4 different miRNAs, namely *MIR155* [38], *MIR15A* [39], *MIR16* [39] and *MIR185* [40] were shown to target RICTOR in an autophagy context. In none of the studies was RICTOR shown as a rate-limiting target for autophagy induction. Moreover, binding regions of these miRNAs in the 3′UTR region of *RICTOR* mRNA were different and non-overlapping with that of the *MIR211* binding region that we have identified (Figure 5(a)). Furthermore, in our hands, none of these miRNAs were shown to be regulated by starvation or MTOR-inhibition (Figure S10), indicating that *MIR211* plays a special and specific role that is different from other *RICTOR*-targeting miRNAs in autophagy control.

Here we showed for the first time, the role of a MITF-specific axis, the MITF-*MIR211* axis, in the control of starvation- and MTOR-inhibition-mediated autophagy. Considering the co-existence of MITF and *MIR211* in various cell lines and tissues, our results suggest that the MITF-*MIR211* axis is a universal determinant of autophagy amplitude under stress conditions.

Materials and methods

Plasmid constructs

The plasmid encoding the control human telomerase (HTR) genomic region (a nontranslated RNA coding for HTR RNA) was used as control for (*MIR-CNT*) [41]. pEGFP-1-N1-MITF-A (38132) [42], pEGFP-N1-TFEB (38119) [42], pRK-5-MYC-RICTOR (11367) [8], pLKO.1-RICTOR shRNA (1853) [34], and LAMP1-RFP (1817) [43] were purchased from Addgene. GFP-LC3 and RFP tandemly tagged LC3 (tfLC3 or RFP-GFP-LC3) were also described [44,45].

For luciferase tests, 3′ UTR segments containing MRE sequences of *RICTOR* and mutant versions were synthesized as sense and antisense linkers. The linker primers were: *RICTOR* primers 5′ CTAGACCTGAAGCATAATCTTA TCAAAGGGATGTTAACT-3′, 5′-CTAGAGTTAACATCC CTTTGATAAGATTATGCTTCAGGT-3′. Mutant *RICTOR* primers 5′-CTAGACCTCTACCAAAATCTTATGTTACCC ATGTTAACT-3′,5′-CTAGAGTTAACATGGGTAACATAAG ATTTTGGTAGAGGT-3′. Double-stranded DNA linkers with added sticky *XbaI* sites were created by annealing complementary strands following incubation at 95°C and slow cooling at RT. Linkers were cloned into the luciferase reporter pGL3-control vector (Promega, E1741) in the 3′ UTR region of the luciferase gene into *XbaI* sites between the stop codon and the polyadenylation signal.

Cell culture and transfection

HeLa cervix cancer cells, HEK293T human embryonic kidney cells and MCF-7 breast cancer cells were cultured in Dulbecco's modified Eagle's medium (DMEM; Biological Industries, BI01-050-1A) supplemented with 10% (v:v) fetal bovine serum (PAN, P30-3302), antibiotics (penicillin/streptomycin; Biological Industries, BI03-031-1B) and L-glutamine (Biological Industries, BI03-020-1B) in a 5% CO_2 humidified incubator at 37°C. The melanoma cell line SK-MEL-28 and breast cancer cell line MDA-MB-231 were cultured in DMEM medium additionally supplemented with 1% non-essential amino acids (Gibco, 11140-035). SHSY-5Y neuroblastoma cells were cultured in fully supplemented DMEM low glucose (1000 mg/l) medium. HeLa and HEK293T cells were transiently transfected using the calcium phosphate method according to standard protocols [46]. SK-MEL-28 and MCF-7 cells were transiently transfected using the polyethylenimine (PolySciences Inc., 23966) transfection method according to Foley et al [47]. Stable RFP-GFP-LC3 HeLa monoclones were created by 4 weeks of G418 (Roche, 04727894001) selection following transfection of cells with the construct. For induction of autophagy, cells were incubated in culture media containing torin1 (200 nM; Tocris, 4247) dissolved in DMSO (Sigma, D2650), or cells were starved in Earle's Balanced Salt solution (Biological Industries, BI02-010-1A) for 4 h. Autophagic flux experiments were performed in the presence or absence of lysosomal protease inhibitors E64D (10 μg/ml; Santa Cruz Biotechnology, SC201280A) and pepstatin A (10 μg/ml; Sigma, P5318) for 4 h.

Immunoblotting and antibodies

Cells were lysed at the indicated time points in RIPA buffer (50 mM TRIS-HCl, pH 7.4, 150 mM NaCl [Applichem, A2942], 1% NP40 [Sigma, 74385], 0.25% Na-deoxycholate [Sigma, 30970]) supplemented with a complete protease inhibitor cocktail (Sigma, P8340) and 1 mM phenylmethylsulfonyl fluoride (Sigma, P7626). Protein extracts (30 μg per well for autophagy assays, and 80 μg per well for MTOR pathway assays) were separated using 6–15% SDS-polyacrylamide gels, and then transferred onto nitrocellulose membranes (Millipore, IPVH00010). Membranes were blocked in 5% nonfat milk (Applichem, A0830) or in 3% BSA (Capricorn, BSA-1T) in PBS-T (3.2 mM Na_2HPO_4[Sigma, S5136], 0.5 mM KH_2PO_4[Sigma, 4243], 1.3 mM KCl[Sigma, P9333], 135 mM NaCl, 0.05% Tween 20[Sigma, P5927], pH 7.4) for 1 h, and then incubated with primary antibodies in a 3% BSA-PBS-T solution. Following PBS-T washes, membranes were incubated with horseradish peroxidase-coupled secondary anti-mouse (Jackson Immunoresearch Laboratories, 115035003) or anti-rabbit (Jackson Immunoresearch Laboratories, 111035144) antibodies. Anti-LC3B (Novus, 2331), anti-RICTOR (Cell Signaling Technology, 2114S), anti-phospho-MTOR (Ser2448; Cell Signaling Technology, 5536), anti-MTOR (Cell Signaling Technology, 2972), anti-RPS6KB/p70S6K (Cell Signaling Technology, 2708), anti-phospho-

RPS6KB/p70S6K (Thr389; Cell Signaling Technology, 9205), anti-AKT (Cell Signaling Technology, 9272S), anti-phospho-AKT (Ser473; Cell Signaling Technology, 587F11), anti-MITF clone 5 (Millipore, MAB3747-I), anti-TFEB (Cell Signaling Technology, 4240), anti-GFP (Roche, 11814460001), anti-ACT/β-ACTIN (Sigma, A5441) or anti-VIM/vimentin (Sigma, V6630) antibodies were used. ImageJ software was used to quantify protein band intensities [48].

Immunofluorescence analyses

Cells were cultured on coverslides and fixed in an ice-cold 4% paraformaldehyde-PBS solution (pH 7.4). For indirect immunostaining experiments, following fixation, cells were permeabilized in PBS containing 0.1% BSA (Sigma, A4503) and 0.1% saponin (Sigma, 84510). As primary antibodies, anti-MITF clone 5, and anti-TFEB were used. Anti-mouse Alexa Fluor 594 (Invitrogen, A11005) and anti-rabbit Alexa Fluor 594 (Invitrogen, A11002) were used as secondary antibodies. When indicated, nuclei were stained using Hoechst dye in 1x PBS. Coverslides were mounted onto glass slides, and samples were analyzed using a BX60 fluorescence microscope (Olympus, BX60).

For experiments with fluorescent protein fusions, cells stably expressing RFP-GFP-LC3 or cells transiently transfected with a plasmid encoding GFP-LC3, RFP-LAMP1, or GFP-MITF-A, GFP-TFEB or GFP-WIPI1 plasmids were used. After 48 h, cells were fixed in ice-cold 4% paraformaldehyde-PBS. Coverslides were then mounted onto glass slides, and samples were analyzed using a BX60 fluorescence microscope (Olympus, BX60) or a Carl Zeiss LSM 710 confocal microscope (Zeiss, Germany).

Quantitative GFP-LC3, GFP-WIPI1, RFP-GFP-LC3, RFP-LAMP1 analyses

Dot counts were performed in RFP-GFP-LC3 stable HeLa cells or GFP-LC3-transfected SK-MEL-28 cells or GFP-WIPI1-transfected HeLa cells. Basal autophagy threshold was determined as 15 GFP-LC3 dots per RFP-GFP-LC3 stable HeLa cell, and 5 GFP-LC3 dots per SK-MEL-28 cell. At least 150 GFP-positive cells per condition were analyzed, and results were expressed as percentage of GFP-LC3 dot-positive cells (above the thresholds) versus total number of transfected cells. For GFP-WIPI1 tests, at least 40 GFP-positive cells per condition were analyzed and quantified by ImageJ analyses, and results were expressed as number of GFP-WIPI1 puncta per cell.

For RFP-GFP-LC3 tests, at least 30 RFP-GFP-positive HeLa cells for each experimental condition were analyzed under a fluorescence microscope (Olympus BX60, Japan) using a 60x magnification. Autophagosomes gave both RFP and GFP signals, while autolysosomes were defined as RFP-positive dots. The number of autolysosomes was calculated by subtracting GFP-positive dot numbers from RFP-positive dot numbers. For GFP-LC3 and RFP-LAMP1 colocalization tests, at least 20 cells for each experimental condition were analyzed under a Carl Zeiss LSM 710 confocal microscope (Zeiss, Germany).

Bioinformatics analyses

miRNA targets were identified using publicly available bioinformatics tools FindTar3 (http://bio.sz.tsinghua.edu.cn), TargetScan Human (www.targetscan.org/), miRanda (www.microrna.org), miRDB (http://mirdb.org/) and RNA22 (cm.jefferson.edu/rna22). Pearson correlation analysis of MITF and *MIR211* expression across NCI-60 cell lines was performed using bioinformatic tools available on the CellMiner website (https://discover.nci.nih.gov/cellminer/analysis.do). Detailed information on multiple platform analysis tools were previously published [49]. For TCGA analyses (http://cancergenome.nih.gov/), datasets of MITF and *MIR211* expression were downloaded using FireBrowse RESTful API (http://firebrowse.org/api-docs/). Datasets were selected according to the following criteria: (i) the number of samples that have missing values for *MIR211* expression less than 40% of all samples; and (ii) the number of samples with both MITF and *MIR211* expression larger than 100. Pearson correlation analyses were performed using datasets meeting the criteria above: Skin Cutaneous Melanoma, Glioma, Pan-kidney Cohort, Testicular Germ Cell Tumors, and Ovarian Serous Cystadenocarcinoma.

RNA isolation and RT-PCR analyses

Total RNA was extracted using TRIzol reagent (Sigma, T9424) according to the manufacturer's instructions. cDNA was reverse transcribed from DNase 1 (Thermo Fischer Scientific, EN0521)-treated total RNA using M-MuLV reverse transcriptase (Fermentas, EP0351) and random hexamers (Invitrogen, 48190-011). For real-time RT-PCR quantification of mRNA levels, the SYBR Green Quantitative RT-PCR kit (Roche, 04-913-914-001) and LightCycler 480 (Roche) were used. To activate the SYBR Green, an initial cycle of 95°C, 10 min was performed. PCR reactions were as follows: 95°C for 15 sec and 60°C for 1 min. (40 cycles). Then a thermal denaturation protocol was used to generate the dissociation curves for the verification of amplification specificity (a single cycle of 95°C for 60 sec, 55°C for 60 sec and 80 cycles of 55°C for 10 sec). Changes in mRNA levels were quantified using the $2^{-\Delta\Delta CT}$ method using *GAPDH* (glyceraldehyde-3-phosphate dehydrogenase) mRNA as control. Primers used were: *RICTOR* primers 5′-AGTGAATCTGTGCCATCGAGT −3′, 5′-AGTAGAGCTGCTGCCAAACC −3′; Pan-*MITF* primers 5′-TTCACGAGCGTCCTGTATGCAGAT-3′, 5′-TTGCAAAGCAGGATCCATCAAGCC-3′; *MITF-M* primers 5′-TCTACCGTCTCTCACTGGATTGG-3′, 5′-GCTTTACCTGCTGCCGTTGG-3′; *MITF-A* primers 5′-GCAGTGGAAGGACGGGAAG-3′, 5′-CAGGATGCTCGGCGGAAC-3′; *ATG10* primers 5′- GTCACATCTAGGAGCATCTACCC-3′, 5′-CATCCAAGGGTAGCTCGAAA-3′; *LC3B* primers 5′-GAGAAGCAGCTTCCTGTTCTGG-3′, 5′-GTGTCCGTTCACCAACAGGAAG-3′; *GAPDH* primers 5′-AGCCACATCGCTCAGACAC-3′, 5′-GCCCAATACGACCAAATCC-3′; *MIR155* stem-loop primer, 5′-GTCGTATCCAGTGCAGGGTCCGAGGTATTCGCACTGGATACGACACC-CCTA-3′, *MIR155* forward primer, 5′-GTTGGGTTAATGCTAATCGTGA-3′; *MIR15A* stem-loop primer, 5′-

GTCGTATCCAGTGCAGGGTCCGAGGTATTCGCACT GGATACGACCACAAAC-3′, *MIR15A* forward primer, 5′-GGGTAGCAGCACATAATG-3′; *MIR16* stem-loop primer, 5′-GTCGTATCCAGTGCAGGGTCCGAGGTATTCGCACT GGATACGACCGCCAAT-3′, *MIR16* forward primer, 5′-GTTTGGTAGCAGCACGTAAAT-3′; *MIR185* stem-loop primer, 5′-GTCGTATCCAGTGCAGGGTCCGAGGTATTCGC ACTGGATACGACTCAGGAA-3′, *MIR185* forward primer, 5′-GTGTGGAGAGAAAGGCAG-3′; Universal reverse primer, 5′-GTGCAGGGTCCGAGGT-3′. TaqMan RT-qPCR reactions were performed using FastStart Universal Probe Master kit (Roche, 04913957001) and LightCycler 480 according to previously described protocols [24]. Primers and the probe used during the study were: *MIR211* stem-loop primer, 5′- GTCGTATCCAGTGCAGGGTCCGAGGTATTCGCACT GGATACGACAGGCGA-3′; *MIR211* forward primer, 5′-GGGTTCCCTTTGTCATCCT-3′; Universal reverse primer, 5′-GTGCAGGGTCCGAGGT-3′; *MIR211* TaqMan Probe, 5′-(6-FAM)-CGCACTGGATACGACAGGCGAAG-(TAMRA-sp)-3′.

Dual luciferase-reporter assay

Luciferase vectors containing wild-type or mutant *MIR211* MREs from the *RICTOR* 3′ UTR were co-transfected with *MIR211* or *ANT211* and a Renilla luciferase construct into HeLa and SK-MEL-28 cells. HEK293T cells were co-transfected with *MIR211* and a Renilla luciferase construct. After 48 h, cells were lysed. Firefly and Renilla luciferase activities were measured using a dual luciferase-reporter assay system (Promega, E1910) and a luminometer (Thermo Fischer Scientific, Fluoroskan Ascent FL). Results were calculated following normalization of the firefly luciferase activity to the renilla luciferase activity.

Antagomir and siRNA tests

miRIDIAN microRNA Hairpin Inhibitors (antagomirs) against *MIR211* (hsa-*MIR211*, IH-300566-05-0005) and a control antagomir (miRIDIAN microRNA hairpin inhibitor negative control, IN001005-01-05) were purchased from Dharmacon. The control antagomir sequence was based on *miR-67 C. elegans* microRNA which has minimal sequence similarity with known human miRNAs. Transfection of antagomirs (200 nM per point) was performed using either the polyethylenimine transfection or calcium phosphate protocols as previously explained [23]. Pan-*MITF* siRNA (siGenome SMARTPool human *MITF* siRNA, M-008674–00-0005) and control siRNA (D-001210–01-20) were purchased from Dharmacon, and 40 nM/well siRNA was transfected.

Chromatin immunoprecipitation (ChIP) and ChIP-qPCR

For ChIP, HeLa and SK-MEL-28 cells were cultured for 48 h and either incubated for 4 h with DMSO or torin1 (200 nM) and subsequently crosslinked in 1% formaldehyde (Sigma, F8775) at room temperature for 10 min. Fixation was stopped by adding 125 mM glycine (Applichem, A1067). Cells were then harvested and lysed in 2 ml of ChIP lysis buffer (50 mM HEPES [Sigma, 54457], 150 mM NaCl, 1% Triton X-100 [Applichem, A4975], 0.1% Na-deoxycholate, 1 mM EDTA [Calbiochem, 324503] containing 0.25% SDS [Applichem, A2572] and protease inhibitor cocktail [Sigma, P8340]). The lysates were subjected to sonication to shear DNA to the length of approximately 150–900 base pairs using a Q700 Sonicator (QSonica). An aliquot (20%) of the supernatant fraction from the chromatin was used as the 'input sample'. For IP, MITF antibody (5 µg/sample; Millipore, MAB3747-I) was incubated with 50 µL of protein-G Dynabeads (Invitrogen, 10003D) overnight at 4°C and washed 3 times with ChIP lysis buffer containing protease inhibitor cocktail. A fraction (500 µg) of the resulting sheared chromatin samples were incubated with MITF antibody-coupled magnetic beads or with beads only (for background control) for 2 h at room temperature. Beads were washed 2x with ChIP lysis buffer, 2x with high salt wash buffer (ChIP lysis buffer containing 500 mM NaCl) and 2x with Tris-EDTA (10 mM Tris-Cl, 1 mM EDTA, pH 8). Immunocomplexes were eluted using 100 µL Tris-EDTA at 95°C for 10 min. After elution, crosslink was reversed by adding NaCl of 200 mM final concentration and incubated with proteinase K (Thermo Fisher Scientific, EO0491) overnight at 65°C. DNA fragments were purified by phenol-chloroform extraction, air-dried, and redissolved in H_2O. Quantitative real-time PCR was performed using a SYBR Green Quantitative RT-PCR kit (Roche, 04-913-914-001) and a LightCycler 480. Primers used were: *MIR211* promoter-specific primers, 5′-CATCGCTTCACAGCAATCATGAGG-3′, 5′-ATCTGAGCTTACCTGCCACAGCA-3′;*LC3B* promoter-specific primers, 5′-CATGCC TTGGGACACCAGAT-3′, 5′-ACCTTCTTCAAGTGCTGTTTGT-3′; *HSPA/HSP70* promoter-specific primers, 5′-CCTCCAGTGA ATCCCAGAAGACTCT-3′, 5′-TGGGACAACGG GAGTCACTCTC-3′. The results are presented as percentage of input.

Human tissue samples

Human tissue sample collection and experiments were conducted in accordance with the guidelines set by the Turkish Republic Ministry of Health, and approved by the Ethics Committee of Dr. Sadi Konuk Research and Training Hospital and Sabanci University. Samples were drop frozen in liquid nitrogen shortly after admission of cadavers to the Council of Forensic Medicine. RNA isolation and protein analyses were performed from frozen tissue powders according to the protocols above.

Statistical analyses

Statistical analyses were performed using Student's two-tailed t-test. Data were represented as means of ± SD of n

independent experiments (biological replicates). Values of $p < 0.05$ were considered as significant.

Acknowledgments

This work was supported by the Scientific and Technological Research Council of Turkey (TUBITAK) 1001 grant number 112T272 and Sabanci University. D.G. is a recipient of an EMBO Strategical Development and Installation Grant (EMBO-SDIG), Turkish Academy of Sciences (TUBA) GEBIP Award, IKU Prof. Dr. Onder Oztunali Science Award, TGC Sedat Simavi Health Sciences Award and Elginkan Foundation Technology Award. shRICTOR (Addgene, 1853) and MYC-RICTOR (Addgene, 11367) plasmids were kindly provided by David Sabatini. pEGFP-N1-TFEB (Addgene, 38119), pEGFP-N1-MITF-A (Addgene, 38132) constructs were kindly provided by Shawn Ferguson. RFP-LAMP1 (Addgene, 1817) was kindly provided by Walther Mothes. The SK-MEL-28 cell line was a kind gift of N.C. Tolga Emre, Bogazici University. We also thank N. C. Tolga Emre for providing us ChIP protocol. We thank Nur M. Kocaturk who kindly helped and assisted with the confocal microscopy analysis. The authors declare that they have no conflict of interest.

Disclosure statement

No potential conflict of interest was reported by the authors.

Funding

This work was supported by the TUBITAK [112T272].

ORCID

Devrim Gozuacik http://orcid.org/0000-0001-7739-2346

References

[1] Mizushima N. Autophagy: process and function. Genes Dev. 2007 Nov 15;21(22):2861–2873. PubMed PMID: 18006683.
[2] Gozuacik D, Kimchi A. Autophagy as a cell death and tumor suppressor mechanism. Oncogene. 2004 Apr 12;23(16):2891–2906. PubMed PMID: 15077152.
[3] Oral O, Akkoc Y, Bayraktar O, et al. Physiological and pathological significance of the molecular cross-talk between autophagy and apoptosis. Histol Histopathol. 2016 May;31(5):479–498. PubMed PMID: 26680630.
[4] Hosokawa N, Hara T, Kaizuka T, et al. Nutrient-dependent MTORC1 association with the ULK1-Atg13-FIP200 complex required for autophagy. Mol Biol Cell. 2009 Apr;20(7):1981–1991. PubMed PMID: 19211835; PubMed Central PMCID: PMCPMC2663915.
[5] Erbil S, Oral O, Mitou G, et al. RACK1 is an interaction partner of ATG5 and a novel regulator of autophagy. J Biol Chem. 2016 Aug 5;291(32):16753–16765. PubMed PMID: 27325703; PubMed Central PMCID: PMCPMC4974388.
[6] Hara K, Maruki Y, Long X, et al. Raptor, a binding partner of target of rapamycin (TOR), mediates TOR action. Cell. 2002 Jul 26;110(2):177–189. PubMed PMID: 12150926.
[7] Saxton RA, Sabatini DM. MTOR signaling in growth, metabolism, and disease. Cell. 2017 Apr 6;169(2):361–371. PubMed PMID: 28388417.
[8] Sarbassov DD, Ali SM, Kim DH, et al. Rictor, a novel binding partner of MTOR, defines a rapamycin-insensitive and raptor-independent pathway that regulates the cytoskeleton. Curr Biol. 2004 Jul 27;14(14):1296–1302. PubMed PMID: 15268862.
[9] Oh WJ, Jacinto E. MTOR complex 2 signaling and functions. Cell Cycle. 2011 Jul 15;10(14):2305–2316. PubMed PMID: 21670596; PubMed Central PMCID: PMCPMC3322468.
[10] Liu P, Gan W, Chin YR, et al. PtdIns(3,4,5)P3-dependent activation of the MTORC2 kinase complex. Cancer Discov. 2015 Nov;5(11):1194–1209. PubMed PMID: 26293922; PubMed Central PMCID: PMCPMC4631654.
[11] Inoki K, Ouyang H, Zhu T, et al. TSC2 integrates Wnt and energy signals via a coordinated phosphorylation by AMPK and GSK3 to regulate cell growth. Cell. 2006 Sep 08;126(5):955–968. PubMed PMID: 16959574.
[12] Sancak Y, Peterson TR, Shaul YD, et al. The Rag GTPases bind raptor and mediate amino acid signaling to MTORC1. Science. 2008 Jun 13;320(5882):1496–1501. PubMed PMID: 18497260; PubMed Central PMCID: PMCPMC2475333.
[13] Laplante M, Sabatini DM. MTOR signaling at a glance. J Cell Sci. 2009 Oct 15;122(Pt 20):3589–3594. PubMed PMID: 19812304; PubMed Central PMCID: PMCPMC2758797.
[14] Kim E, Goraksha-Hicks P, Li L, et al. Regulation of TORC1 by Rag GTPases in nutrient response. Nat Cell Biol. 2008 Aug;10(8):935–945. PubMed PMID: 18604198; PubMed Central PMCID: PMCPMC2711503.
[15] Martina JA, Puertollano R. Rag GTPases mediate amino acid-dependent recruitment of TFEB and MITF to lysosomes. J Cell Biol. 2013 Feb 18;200(4):475–491. PubMed PMID: 23401004; PubMed Central PMCID: PMCPMC3575543.
[16] Perera RM, Stoykova S, Nicolay BN, et al. Transcriptional control of autophagy-lysosome function drives pancreatic cancer metabolism. Nature. 2015 Aug 20;524(7565):361–365. PubMed PMID: 26168401; PubMed Central PMCID: PMCPMC5086585.
[17] Palmieri M, Impey S, Kang H, et al. Characterization of the CLEAR network reveals an integrated control of cellular clearance pathways. Hum Mol Genet. 2011 Oct 01;20(19):3852–3866. PubMed PMID: 21752829.
[18] Ploper D, Taelman VF, Robert L, et al. MITF drives endolysosomal biogenesis and potentiates Wnt signaling in melanoma cells. Proc Natl Acad Sci U S A. 2015 Feb 03;112(5):E420–9. PubMed PMID: 25605940; PubMed Central PMCID: PMCPMC4321275.
[19] Martina JA, Diab HI, Lishu L, et al. The nutrient-responsive transcription factor TFE3 promotes autophagy, lysosomal biogenesis, and clearance of cellular debris. Sci Signal. 2014 Jan 21;7(309):ra9. PubMed PMID: 24448649; PubMed Central PMCID: PMCPMC4696865.
[20] Settembre C, Di Malta C, Polito VA, et al. TFEB links autophagy to lysosomal biogenesis. Science. 2011 Jun 17;332(6036):1429–1433. PubMed PMID: 21617040; PubMed Central PMCID: PMCPMC3638014.
[21] Ozturk DG, Kocak M, Gozuacik D. Cloning of autophagy-related MicroRNAs. Methods Mol Biol. 2017 Oct 12. PubMed PMID: 29022289. DOI:10.1007/7651_2017_83.
[22] Gozuacik D, Akkoc Y, Ozturk DG, et al. Autophagy-regulating microRNAs and cancer. Front Oncol. 2017;7:65. PubMed PMID: 28459042; PubMed Central PMCID: PMCPMC5394422.
[23] Korkmaz G, le Sage C, Tekirdag KA, et al. miR-376b controls starvation and MTOR inhibition-related autophagy by targeting ATG4C and BECN1. Autophagy. 2012 Feb 1;8(2):165–176. PubMed PMID: 22248718.
[24] Korkmaz G, Tekirdag KA, Ozturk DG, et al. MIR376A is a regulator of starvation-induced autophagy. PLoS One. 2013;8(12):e82556. PubMed PMID: 24358205; PubMed Central PMCID: PMCPMC3864973.
[25] Tekirdag KA, Akkoc Y, Kosar A, et al. MIR376 family and cancer. Histol Histopathol. 2016 Aug;31(8):841–855. PubMed PMID: 26940843.
[26] Sardiello M, Palmieri M, di Ronza A, et al. A gene network regulating lysosomal biogenesis and function. Science. 2009 Jul 24;325(5939):473–477. PubMed PMID: 19556463.
[27] Napolitano G, Ballabio A. TFEB at a glance. J Cell Sci. 2016 Jul 01;129(13):2475–2481. PubMed PMID: 27252382; PubMed Central PMCID: PMCPMC4958300.
[28] Bouche V, Espinosa AP, Leone L, et al. Drosophila Mitf regulates the V-ATPase and the lysosomal-autophagic pathway. Autophagy.

2016;12(3):484–498. PubMed PMID: 26761346; PubMed Central PMCID: PMCPMC4835958.

[29] Settembre C, Zoncu R, Medina DL, et al. A lysosome-to-nucleus signalling mechanism senses and regulates the lysosome via MTOR and TFEB. Embo J. 2012 Mar 07;31(5):1095–1108. PubMed PMID: 22343943; PubMed Central PMCID: PMCPMC3298007.

[30] Proikas-Cezanne T, Ruckerbauer S, Stierhof YD, et al. Human WIPI-1 puncta-formation: a novel assay to assess mammalian autophagy. FEBS Lett. 2007 Jul 24;581(18):3396–3404. PubMed PMID: 17618624.

[31] Klionsky DJ, Abdelmohsen K, Abe A, et al. Guidelines for the use and interpretation of assays for monitoring autophagy (3rd edition). Autophagy. 2016;12(1):1–222. PubMed PMID: 26799652; PubMed Central PMCID: PMCPMC4835977.

[32] Miller AJ, Du J, Rowan S, et al. Transcriptional regulation of the melanoma prognostic marker melastatin (TRPM1) by MITF in melanocytes and melanoma. Cancer Res. 2004 Jan 15;64(2):509–516. PubMed PMID: 14744763.

[33] Mazar J, DeYoung K, Khaitan D, et al. The regulation of miRNA-211 expression and its role in melanoma cell invasiveness. PLoS One. 2010 Nov 1;5(11):e13779. PubMed PMID: 21072171; PubMed Central PMCID: PMCPMC2967468.

[34] Sarbassov DD, Guertin DA, Ali SM, et al. Phosphorylation and regulation of Akt/PKB by the rictor-MTOR complex. Science. 2005 Feb 18;307(5712):1098–1101. PubMed PMID: WOS:000227197300045; English.

[35] Hartman ML, Czyz M. MITF in melanoma: mechanisms behind its expression and activity. Cell Mol Life Sci. 2015 Apr;72(7):1249–1260. PubMed PMID: 25433395; PubMed Central PMCID: PMCPMC4363485.

[36] Levy C, Khaled M, Iliopoulos D, et al. Intronic miR-211 assumes the tumor suppressive function of its host gene in melanoma. Mol Cell. 2010 Dec 10;40(5):841–849. PubMed PMID: 21109473; PubMed Central PMCID: PMCPMC3004467.

[37] Ozeki N, Hase N, Hiyama T, et al. MicroRNA-211 and autophagy-related gene 14 signaling regulate osteoblast-like cell differentiation of human induced pluripotent stem cells. Exp Cell Res. 2017 Mar 01;352(1):63–74. PubMed PMID: 28159471.

[38] Wan G, Xie W, Liu Z, et al. Hypoxia-induced MIR155 is a potent autophagy inducer by targeting multiple players in the MTOR pathway. Autophagy. 2014 Jan;10(1):70–79. PubMed PMID: 24262949; PubMed Central PMCID: PMCPMC4389881.

[39] Huang N, Wu J, Qiu W, et al. MiR-15a and miR-16 induce autophagy and enhance chemosensitivity of Camptothecin. Cancer Biol Ther. 2015;16(6):941–948. PubMed PMID: 25945419; PubMed Central PMCID: PMCPMC4622988.

[40] Zhou L, Liu S, Han M, et al. MicroRNA-185 induces potent autophagy via AKT signaling in hepatocellular carcinoma. Tumour Biol. 2017 Feb;39(2):1010428317694313. PubMed PMID: 28240051.

[41] Voorhoeve PM, le Sage C, Schrier M, et al. A genetic screen implicates miRNA-372 and miRNA-373 as oncogenes in testicular germ cell tumors. Cell. 2006 Mar 24;124(6):1169–1181. S0092-8674(06)00291-1 [pii], PubMed PMID: 16564011; eng.

[42] Roczniak-Ferguson A, Petit CS, Froehlich F, et al. The transcription factor TFEB links MTORC1 signaling to transcriptional control of lysosome homeostasis. Sci Signal. 2012 Jun 12;5(228):ra42. PubMed PMID: 22692423; PubMed Central PMCID: PMCPMC3437338.

[43] Sherer NM, Lehmann MJ, Jimenez-Soto LF, et al. Visualization of retroviral replication in living cells reveals budding into multivesicular bodies. Traffic. 2003 Nov;4(11):785–801. PubMed PMID: 14617360.

[44] Kimura S, Fujita N, Noda T, et al. Monitoring autophagy in mammalian cultured cells through the dynamics of LC3. Methods Enzymol. 2009;452:1–12. PubMed PMID: 19200872.

[45] Kabeya Y, Mizushima N, Ueno T, et al. LC3, a mammalian homologue of yeast Apg8p, is localized in autophagosome membranes after processing. Embo J. 2000 Nov 1;19(21):5720–5728. PubMed PMID: 11060023; PubMed Central PMCID: PMCPMC305793.

[46] Jordan M, Schallhorn A, Wurm FM. Transfecting mammalian cells: optimization of critical parameters affecting calcium-phosphate precipitate formation. Nucleic Acids Res. 1996 Feb 15;24(4):596–601. PubMed PMID: 8604299; PubMed Central PMCID: PMCPMC145683.

[47] Foley CJ, Freedman H, Choo SL, et al. Dynamics of RASSF1A/MOAP-1 association with death receptors. Mol Cell Biol. 2008 Jul;28(14):4520–4535. PubMed PMID: 18474619; PubMed Central PMCID: PMCPMC2447132.

[48] Abràmoff MD, Magalhães PJ, Ram SJ. Image processing with ImageJ. Biophotonics Int. 2004;11(7):36–42.

[49] Reinhold WC, Sunshine M, Liu H, et al. CellMiner: a web-based suite of genomic and pharmacologic tools to explore transcript and drug patterns in the NCI-60 cell line set. Cancer Res. 2012 Jul 15;72(14):3499–3511. PubMed PMID: 22802077; PubMed Central PMCID: PMCPMC3399763.